A CONTINUOUS WAVE, SINGLE FREQUENCY INTRACAVITY OPTICAL PARAMETRIC OSCILLATOR BASED UPON THE TWISTED-MODE TECHNIQUE

Lea Christina Heering

A Thesis Submitted for the Degree of MPhil
at the
University of St Andrews

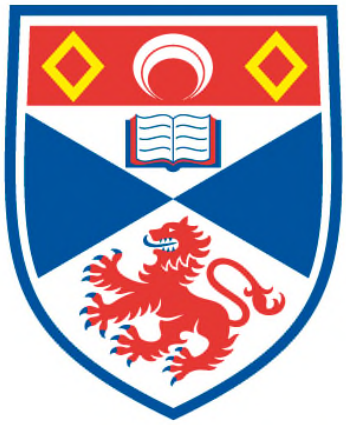

2014

A continuous wave, single frequency Intracavity Optical Parametric Oscillator based upon the Twisted-Mode Technique

Lea Christina Heering

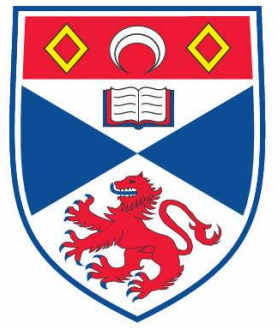

This thesis is submitted in partial fulfilment for the degree of MPhil
at the
University of St Andrews

31st March 2014

1. Candidate's declarations:

I, Lea Christina Heering hereby certify that this thesis, which is approximately 12500 words in length, has been written by me, that it is the record of work carried out by me and that it has not been submitted in any previous application for a higher degree.

I was admitted as a research student in August, 2012 and as a candidate for the degree of MPhil in August, 2012; the higher study for which this is a record was carried out in the University of St Andrews between 2012 and 2014.

Date: ..... signature of candidate .....

2. Supervisor's declaration:

I hereby certify that the candidate has fulfilled the conditions of the Resolution and Regulations appropriate for the degree of MPhil in the University of St Andrews and that the candidate is qualified to submit this thesis in application for that degree.

Date: ..... signature of supervisor .....

3. Permission for electronic publication:

In submitting this thesis to the University of St Andrews I understand that I am giving permission for it to be made available for use in accordance with the regulations of the University Library for the time being in force, subject to any copyright vested in the work not being affected thereby. I also understand that the title and the abstract will be published, and that a copy of the work may be made and supplied to any bona fide library or research worker, that my thesis will be electronically accessible for personal or research use unless exempt by award of an embargo as requested below, and that the library has the right to migrate my thesis into new electronic forms as required to ensure continued access to the thesis. I have obtained any third-party copyright permissions that may be required in order to allow such access and migration, or have requested the appropriate embargo below.

The following is an agreed request by candidate and supervisor regarding the electronic publication of this thesis:

(iii) Embargo on both of printed copy and electronic copy for the same fixed period of 1 year on the following ground(s):

publication would be commercially damaging to the researcher, or to the supervisor, or the University; publication would preclude future publication;

Date: ..... signature of supervisor .....

signature of candidate .....

Acknowledgments

First and foremost I would like to thank Malcolm Dunn for giving me the opportunity to complete an MPhil project as part of his research group and for supporting me every step of the way. I am sure he must be the most caring, kind-hearted and inspiring supervisor of all time.

Thank you also to David Stothard and Tom Edwards, who have both helped me enormously over the past year and especially over the last few weeks. Your support and guidance have been absolutely invaluable.

Abstract:

This document summarises a study into the elimination of spatial hole burning in the pump field of a Nd:YAG and PPLN based Intracavity Optical Parametric Oscillator (ICOPO), using the so-called 'twisted-mode technique'. This approach relies on the manipulation of circulating field polarisation to achieve a spatially uniform electric field intensity throughout the laser gain material, thus removing the root of multi-longitudinal-mode oscillation in homogeneously broadened systems. During the course of this investigation the 'twisted-mode' technique was first applied to a basic 1μm Nd:YAG laser, where it proved very successful in facilitating single frequency operation. The laser cavity was then extended to accommodate the ICOPO, which delivered 93.9mW of mid-IR output for 3W of diode pump power. The implementation of the 'twisted-mode' technique was not found to have any significant impact on power performance of the device and once again offered substantial improvements in pump field spectral quality. Although the insertion of an etalon was necessary to achieve good frequency control, the associated drop in power was minimal compared to typical losses observed in etalon-narrowed standing-wave configurations. This can be attributed to both the low finesse that was required as well as the absence of gain unsaturated regions within the active medium, as would be observed in a spatially hole burnt system. Whilst further work will have to be carried out to optimise both the frequency behaviour and power performance of the device, the 'twisted-mode' technique shows clear potential as an approach to the development of a reliable, narrow line-width mid-IR spectroscopic source based on Intracavity OPO technology.

Chapter One

Chapter Two

Chapter Three

Chapter Four

Chapter Five

Chapter One: Introduction

1.1 Introduction to Laser Spectroscopy

With unprecedented spectral brightness, minimal divergence and impressive coherence length, the laser is an ideal source for spectroscopic applications and laser absorption spectroscopy has become a very well-established tool in the detection and identification of a wide range of compounds, owing to the tremendous variety of reliable, efficient laser sources covering the visible as well as the near-infrared bands of the Electromagnetic Spectrum that are readily available today. However, spectroscopic sources emitting over the mid-infrared wavelength range (3-4μm) are still underdeveloped in comparison. Unfortunately, this wavelength range is also arguably one of the most spectroscopically valuable, since it contains key absorption features of many harmful or interesting compounds, notably the hydrocarbons. Thus an extensive number of applications, ranging from pollution detection to medical diagnosis and even quality control in wines, would benefit from the realisation of an ideal mid-IR spectroscopic source. Such a source should exhibit high output powers (10s of mW) to enable long range detection, a narrow linewidth (less than 10 MHz) for the distinction between compounds with similar absorption features, wide (100's nm) and smooth (100's GHz) tuneability for the detection of multiple compounds with a single device, a compact and robust design suitable for applications in the field and low power requirements to make battery operation a possibility [1]. In this investigation we explore one technology which shows considerable potential in meeting the above criteria.

1.2 Mid-Infrared Laser Sources

Let us first consider the current state-of-the-art through an overview of existing technologies and their shortfalls.

1.2.1 Lead Salt Diode Lasers

In the years following the demonstration of the first diode laser by Hall et al. in 1962 (a semiconductor laser based on GaAs) [2] this new technology was implemented using a wide variety of semiconductor materials, resulting in operation wavelengths from the deep infrared all the way up to the ultra-violet. The mid-IR range is covered by a family of materials known as the lead salts [3]. While lead salt diode-based mid-IR spectrometers have been demonstrated [4], [5], these lasers unfortunately still require cryogenic cooling and exhibit very poor spatial mode quality as well as low output powers [6]. Furthermore, the tuning range of lead salt diodes is dictated by the band-gap within the semiconductor material and is therefore limited to ~10s of nm.

1.2.2 Quantum Cascade Lasers

These semiconductor injection lasers have enjoyed by far the greatest research effort in the quest for a mid-IR spectroscopic source. Tremendous progress has been made in this area especially in recent years. Rather than using a single bulk semiconductor material in the optically active region (as is the case in diode lasers), thin layers of various semiconductor materials are stacked on top of each other periodically. When a voltage is applied to this structure, a split of energy levels into 'sub-bands' occurs, creating a 'cascade of quantum wells'. If the semiconductor layers are chosen wisely, a population inversion can be achieved between adjacent sub-band regions, which initiates laser operation. It can therefore be seen that the emission wavelength of a QC laser is only dependent on the thickness of semiconductor layers and can thus be engineered to align with demands by choosing an appropriate thickness. A further advantage of this technology over more traditional semiconductor lasers is that once an electron has crossed the energy band-gap and emitted a photon in one quantum well of the active region, it can tunnel through to the next well and repeat the process as illustrated in Figure 1. This leads to significantly increased output powers. While the first QC laser, built by Faist et al. in 1994 [7], exhibited a wall plug efficiency of just 0.15%, operating at 10K in the pulsed regime, today CW QC lasers are available with

efficiencies as high as 21% at room temperature [8]. It has to be said however, that such efficiencies can only be achieved in low power devices, due to a tendency of these systems to rapidly overheat at high pumping rates. Furthermore, while tuning ranges have been increased significantly by incorporating an array of QC lasers on a single chip and the highest observed tuning range is a respectable 1.8 microns [9], this was achieved in a system with an inhomogeneously broadened gain bandwidth, which was thus operating on multiple cavity modes simultaneously. Tuning ranges within single longitudinal mode QC lasers are still limited [10].

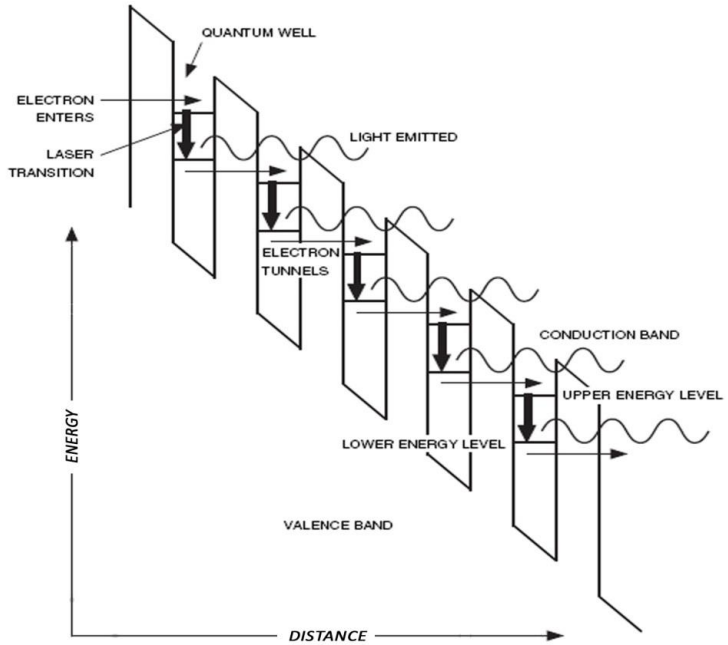

Figure 1.Schematic operation of a Quantum-Cascade Laser.

1.2.3 The Optical Parametric Oscillator (OPO)

It was realised as early as 1928 that it was possible to change the wavelength of light [11]. If light of sufficient intensity were to be passed through a material exhibiting certain nonlinear optical properties, its photons (hereafter *pump* photons) would be split into two photons of lower energy (hereafter the *signal* and *idler*), such that the sum of the frequencies of the generated signal and idler photons add up to the frequency of the original pump photon, the ratio of the split being dependent on phase matching

conditions. It was however not until the demonstration of the laser in 1960, that this knowledge translated into a realistic research prospect, due to the high light intensities required for this process, known as Optical Parametric Generation (OPG), to occur. The first OPO was finally realised by Giordmaine and Miller in 1965 [12], operating in the pulsed regime. A continuous-wave version was developed in 1968 by Smith et al. [13]. The invention of the laser diode revolutionised laser (and with it OPO) technology, as these devices enabled the efficient and relatively compact optical pumping of solid-state lasers, today one of the most well understood, reliable and heavily used category of lasers. The 1990s brought the development of novel nonlinear materials such as periodically poled $LiNbO_3$ (PPLN), which enabled a new and more efficient method of phase-matching, called quasi-phase-matching, to be employed [14] (more on this in Chapter 2). Furthermore these new materials enabled the growth of significantly longer crystals than previously possible and exhibited a greatly superior nonlinear coefficient. These developments led to the advent of a new generation of OPOs with improved efficiency and spectral coverage. The OPO has been demonstrated using a range of cavity designs (see Figure 2), each of which exhibits different threshold and stability requirement characteristics. In the Doubly-Resonant Oscillator (DRO) both of the down-converted waves are resonant. While this significantly reduces power requirements to reach OPO threshold, the DRO cavity length has to be stable to around 1 nm (having to hold two different frequencies on resonance simultaneously) and is thus very sensitive to mechanical perturbation as well as notoriously difficult to tune. The Singly-Resonant Oscillator (SRO) on the other hand is a very stable device, since only one of the down-converted waves is resonant. However, with only one high intensity field passing through the nonlinear crystal, threshold requirements are increased in this system. A compromise is reached in the Pump-Enhanced Oscillator (PE-SRO) [15]. Here the pump field is resonant as well as one of the down-converted waves. The PE-SRO thus exhibits favourable threshold requirements similar to the DRO. However, while mechanical stability is also certainly improved compared to the DRO, electronic locking is still required, leaving the PE-SRO inferior to the SRO in this respect.

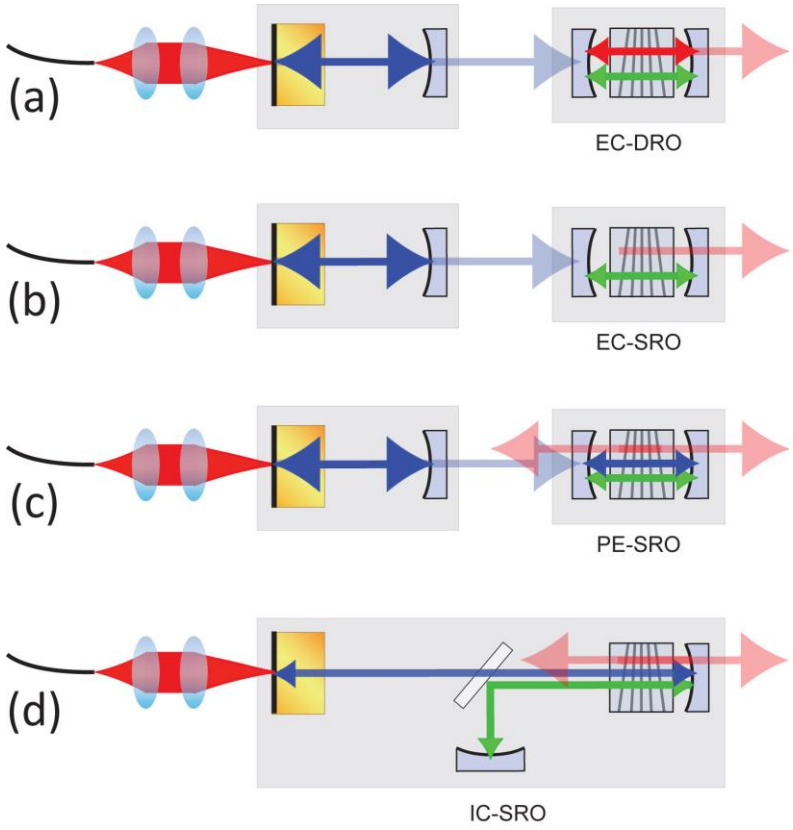

Figure 2: Schematics of OPO cavity configurations, shown in the context of end-pumped solid-state laser-based systems. (a) the Doubly-Resonant Oscillator (DRO), (b) the Singly-Resonant Oscillator (SRO), (c) the Pump-Enhanced, singly-resonant Oscillator (PE-SRO), (d) the Intracavity OPO (ICOPO).
A disadvantage of designs (c) and (d) is a loss of half the idler output, which exits in both directions. Double-passing the idler by HR coating one of the OPO mirrors at idler wavelengths is a possible solution, however avoiding destructive interference would be challenging.

The solution had actually been found by Kroll in 1962 even before the first OPO was demonstrated [16]. By placing the nonlinear crystal *inside* the cavity of the parent pump laser (as shown in Figure 2d), OPO threshold requirements would be reduced dramatically. Resonating both down-converted waves, which leads to stability concerns as outlined above, would thus be unnecessary. In 1996 Colville et al. successfully demonstrated the first cw Intracavity OPO based on a singly-resonant design, here at St Andrews [17]. This pioneering work was undertaken using an Argon-Ion pumped Ti:Sapphire laser which, whilst being an excellent vehicle for such

a study, is an impractical device for use outside the laboratory due to its physical size, complexity and requirement for a high power green pump source.

Configuration	Threshold	Primary Pump Threshold	Stability Comments
DRO	~10mW	~50mW	High stability requirements
SRO	5-10W	10-15W	No stability concerns
PE-SRO	0.5-1W Enhanced to 5-10W	1-2W	Moderate stability requirements
ICOPO	5-10W	300mW-1W	No stability concerns

Table 1: Comparison between OPO cavity designs [18]

In 1998 this was addressed by taking advantage of developments in diode pumped laser technology and nonlinear optical materials in order to realise a highly compact, all solid-state ICOPO based upon Nd:YVO_4 and PPLN [19]. The device, measuring only ~30cm long, exhibited an SRO threshold of just 330mW of primary diode pump power. This technology did however have one significant drawback. The inclusion of a nonlinear crystal within the laser cavity dramatically exacerbated the phenomenon of relaxation oscillations. The interplay between the resonant signal and pump fields given the relatively long upper state lifetime of the Nd:YVO_4 gain medium led to random and long-lived outbursts of oscillatory behaviour of the pump field and thus unacceptable amplitude fluctuations in the idler output, rendering the device useless in terms of spectroscopic applications. In 2009 it was suggested to put a frequency doubling crystal inside the pump cavity, which would systematically and passively smooth out the pump field, due to the amplitude dependant loss introduced. Whilst an attempt was made to implement this idea, the limitations in nonlinear media available at the time prohibited the full suppression of relaxation oscillations, although a

significant improvement was still noted [20]. Finally in 2012, using a PPLN frequency doubling crystal, it was possible to confirm the complete effectiveness of the approach, resulting in the first amplitude stable Nd:YVO_4 based Intracavity OPO [21]. This work was carried out as part of my BSc final year project under the supervision of Malcolm Dunn and David Stothard (see Appendix for a summary of reference). However, due to spatial hole burning in the homogeneously broadened gain medium, the resultant device had a linewidth of ~150 GHz. The frequency spectrum is shown in Figure 3.

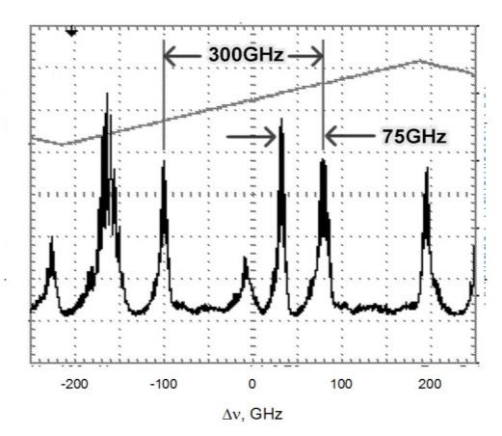

Figure 3: 1 μm light frequency spectrum the Nd:YVO4-based ICOPO built by us in 2012. This trace was taken using a homemade plane-plane Fabry-Perot Interferometer with a FSR of 300 GHz.

Such broad linewidths, whilst being adequate for very crude spectroscopic measurements, are unsuitable for high resolution spectroscopy. Frequency controlling methods would thus have to be employed to realise the full potential of the ICOPO. The next section explores a range of possible strategies.

1.3 Roots to Single Frequency Operation

1.3.1 Intracavity Etalons

A very well established frequency controlling technique is the placement of etalons inside the cavity of a laser resonator. As long as the free spectral ranges of the etalons are well chosen, this is an effective measure for the suppression of multi-mode

behaviour and allows for selection of any particular cavity mode (usually chosen to lie as close to line centre as possible to maximise output). Figure 4 shows the properties of an etalon that would be suitable for mode suppression in the case of the laser output spectrum mentioned in the previous section.

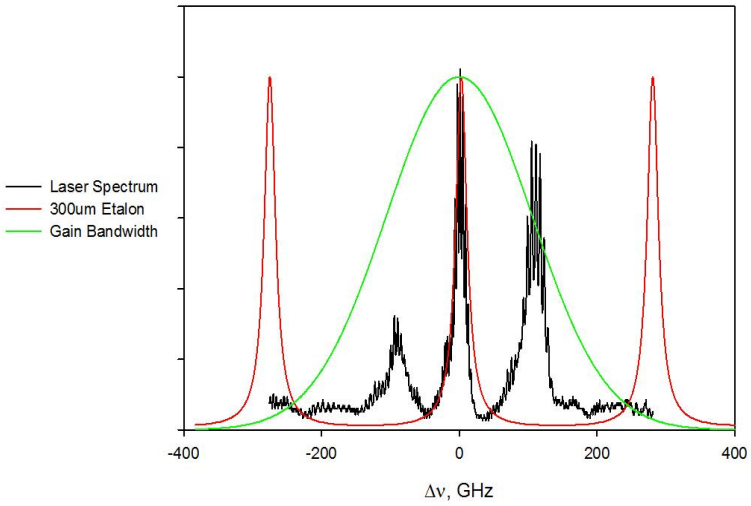

Figure 4: Showing the properties of an etalon well chosen to suppress spatially hole burnt modes in the frequency spectrum shown. This etalon was 300 μm thick with a reflectivity of 80%. The cavity-mode spacing in this system was ~500 MHz.

However, since the optical gain that would have been swept out by the spatially hole burnt modes cannot be utilised by the mode in operation, this gain is left unsaturated and a substantial loss in output power is observed. A 50% drop in idler output was observed in the Nd:YVO_4 system mentioned above, when an etalon was inserted into the pump cavity [21]. Whilst the total output remained reasonable (~75mW of idler for 3W of diode pump), we felt that it was desirable to explore other avenues to single frequency operation, that would not result in such a significant drop in efficiency.

1.3.2 The Ring Laser

Since spatial hole burning is an effect which occurs exclusively in standing wave cavities, a travelling wave cavity configuration eliminates the problem all together. Designing a ring laser is therefore a well-established technique for achieving single frequency operation in homogeneously broadened laser systems and has been

successfully applied to a wide variety of lasers (most notably the Ti:Sapphire). An etalon is still necessary to prevent continuous hopping between cavity modes close to line centre, however a low finesse etalon is usually sufficient and the mode thus selected is able to exploit gain across the entire length of the laser medium, as opposed to being unable to access gain in certain parts of the crystal as is the case in the standing wave configuration. Therefore, the price to be paid for single mode operation is no more than the insertion loss of the etalon, rather than the much more substantial loss sustained in the standing wave design, due to the suppression of spatially hole burnt modes. By employing a 'ring within a ring' design (see Figure 5), Edwards et al. were able to realise the first ring laser pumped ICOPO in 2000, which was based on a Ti:Sapphire source [22]. This technology, whilst very promising, requires a very complex set-up as well as a high-power green pump laser and may thus not be a suitable source for a resilient, light-weight and portable mid-IR spectrometer. Expensive specialist components such as a uni-directional device are also needed, which may increase the price of the finished device to a point where its applications are limited.

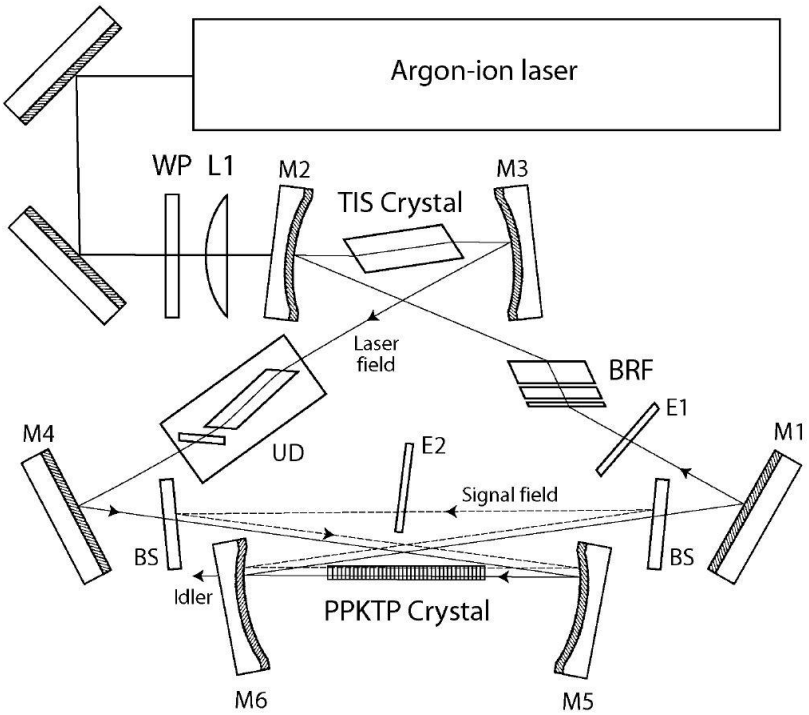

Figure 5: An Intracavity OPO inside the cavity of a Ti:Sapphire laser [22]

1.3.3 The twisted-mode approach

In 1965 Siegman suggested and implemented a novel approach to obtaining single frequency operation in homogeneously broadened laser media that involved manipulation of the polarisation of light passing through the gain material [23]. He inserted a Brewster plate into his Ruby laser cavity to select for a particular linear polarisation. He then placed two quarter-wave plates either side of his gain rod, their fast axes being at 45° to the Brewster plate and at 90° to each other (see Figure 6).

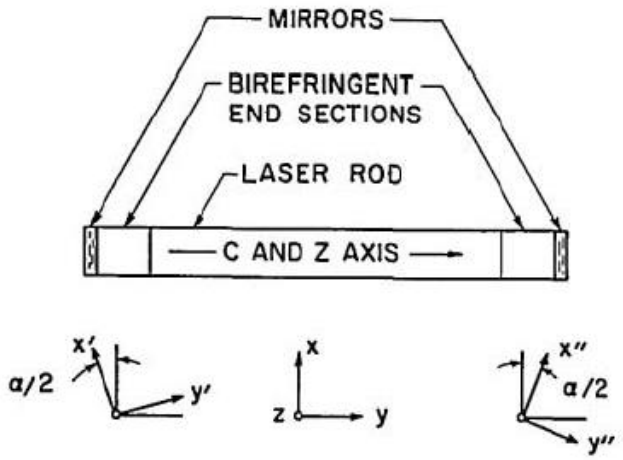

Figure 6: Siegman's twisted-mode set-up, where α denotes the angle between the fast axes of the quarter-wave plates = 90° (from [23])

The first plate would cause light to become circularly polarised on its way through the active medium, while the second would restore the polarisation back to its initial linear state. After bouncing off the end mirror, light would once again pass through a quarter wave plate prior to entering the gain material and have its polarisation changed to circular, this time however with the opposite handedness, before finally a further pass through a plate would once again restore original polarisation. It can be seen that throughout the laser gain medium two oppositely circularly polarised, counter-propagating waves would interact at all times. This would lead to a uniform time-averaged spatial gain density, as opposed to the node and anti-node pattern that is characteristic of linearly polarised standing wave configurations and thus spatial hole burning would be entirely eliminated. Since the success of Siegman's initial

demonstration of the effect the so-called 'twisted-mode' technique has been applied to a wide variety of laser systems over the years. In 1993 such a study was undertaken in the Nonlinear Optics group here at St Andrews [24]. While it was somewhat limited by the low power diode pump sources available at the time, it showed that this approach was viable in the context of a compact Nd:YAG laser. The study was useful to the current investigation since we were able utilise legacy components from the experimental set-up, which enabled us to quickly assess the efficacy of the approach. This is discussed further in Chapter 3.

1.4 Summary and Dissertation Overview

In this chapter we have discussed the need for a narrow line-width, widely tuneable, robust and efficient mid-IR laser source for spectroscopic applications. We briefly considered current state-of-the-art technologies looking to fulfil these requirements and noted their shortfalls. The Intracavity OPO was identified to hold great potential, although frequency selection and control has, to date, proved problematic. The concept of the twisted-mode approach was introduced to address this issue.

In chapter two the underlying theoretical principles of OPOs, spatial hole burning and the twisted-mode technique are explored in more detail. Chapter three describes the realisation and characterisation of a simple Nd:YAG laser using the twisted-mode technique and we will discuss the impact of this approach on frequency behaviour. We then go on to include the Intracavity OPO in chapter four. Finally we summarise the study in chapter five, drawing conclusions and discussing future work.

Chapter Two: Theoretical Background

2.1 The Optical Parametric Oscillator

2.1.1 Origins of Parametric Generation

When an optical field **E** is incident on a dielectric material, the induced oscillating polarization can be expressed by:

$$\boldsymbol{P} = \varepsilon_0[\,\chi^{(1)}\boldsymbol{E} + \chi^{(2)}\boldsymbol{E}^2 + \chi^{(3)}\boldsymbol{E}^3 + \cdots\,] \tag{1}$$

where $\chi^{(1)}$ is the linear susceptibility coefficient of the material, responsible for linear optical phenomena such as refraction and dispersion, in which the re-radiated wave sees no frequency change. $\chi^{(2)}$, $\chi^{(3)}$, ..., denote the higher-order susceptibility coefficients, with the second order nonlinear coefficient ($\chi^{(2)}$) being of particular interest to this investigation since it gives rise to processes such as second harmonic generation (SHG) and parametric generation, the process forming the foundation of OPO operation. High light intensities, as can only be achieved by lasers, are necessary to activate these nonlinear optical processes, since the magnitude of nonlinear susceptibility coefficients decreases rapidly with increasing order.

Let us now consider the second-order nonlinear response of a dielectric material, when two optical fields $\mathbf{E}_1$ and $\mathbf{E}_2$, propagating in the z-direction and oscillating at frequencies ω_1 and ω_2 respectively, are incident simultaneously. The induced second-order polarization can then be described by:

$$\boldsymbol{P}^{(2)} = \varepsilon_0\chi^{(2)}[\boldsymbol{E}_1\cos(k_1z - \omega_1t) + \boldsymbol{E}_2\cos(k_2z - \omega_2t)]^2 \tag{2}$$

This oscillating polarization contains the component:

$$\boldsymbol{P}(\omega_1 - \omega_2) = \frac{1}{2}\varepsilon_0 \chi^{(2)} \boldsymbol{E}_1 \boldsymbol{E}_2 \cos[(k_1 - k_2)z - (\omega_1 - \omega_2)t] \quad (3)$$

The wave re-radiated by this polarization component will have a frequency of $\omega_3 = \omega_1 - \omega_2$, i.e. a new wave has been generated with a frequency equal to the difference between the frequencies of the incident waves, an effect known as frequency-difference mixing. This is the underlying process of parametric generation.

In an OPO a suitable nonlinear material (possessing a high second-order nonlinear susceptibility coefficient) is placed inside a resonator with wavelength specific mirror coatings. The pump field (of frequency ω_2) is provided externally, while the signal field (of frequency ω_1) builds up from parametric noise inside the cavity, provided the gain generated by the pump field is sufficient to overcome the round-trip losses of the cavity. The interaction between the two fields then initiates parametric generation, which yields the idler field (of frequency ω_3). This in turn mixes back with the pump field to amplify the initially weak signal field. In this manner total depletion of the pump field can be achieved, a desirable condition as we will discover later on.

2.1.2 Phase Matching

As we have already seen parametric generation occurs due to the coupled interactions of pump, signal and idler fields inside a suitable nonlinear material and is governed by the relationship:

$$\omega_p = \omega_s + \omega_i \quad (4)$$

The pump field is provided externally and is thus of fixed frequency. However, what determines which signal/idler pair is able to oscillate, given the usually substantial number of possible combinations within the nonlinear material's transparency range?

Making its way through a dielectric material, such as a nonlinear crystal, an optical field will encounter and interact with many polarisation dipoles. In an OPO

configuration it is crucial to ensure that parametric contributions from each dipole are in phase with one another to facilitate constructive interference. The energy transfer between the pump, signal and idler fields inside an OPO can be described by three coupled wave equations, which are obtained by solving Maxwell's wave equation in the presence of the three fields propagating in the z-direction in a second-order nonlinear material [25]:

$$\frac{dE_i}{dt} = i\kappa_i E_p E_s^* e^{i\Delta kz} \tag{5}$$

$$\frac{dE_s}{dt} = i\kappa_s E_p E_i^* e^{i\Delta kz} \tag{6}$$

$$\frac{dE_p}{dt} = i\kappa_p E_i E_s e^{-i\Delta kz} \tag{7}$$

Where E_i, E_s and E_p are complex amplitudes of the idler, signal and pump field, $\kappa_i = [\omega\chi^{(2)}/2n_i c]$, with n_i being the refractive index experienced by the idler field and $\Delta k = k_p - k_s - k_i$ is the so-called phase-mismatch parameter. The general solution of the coupled wave equations is well beyond the scope of this study [26], but let us for simplicity assume that the pump field is not significantly depleted on its way through the parametric gain medium, i.e. $dE_p/dt = 0$. This is a reasonable assumption to make in the case of the Intracavity OPO, where on a single pass through the nonlinear crystal the pump field will be depleted by only a few percent at most. In this case only equations 1 and 2 remain to be considered. It can then be shown that in the case of non-zero signal input field and zero input idler field, the fractional increase in signal field intensity upon propagation through the parametric gain material is given by [27]:

$$G_s(l) = \Gamma^2 l^2 \frac{sinh^2[\Gamma^2 l^2 - \left(\frac{\Delta kl}{2}\right)^2]^{1/2}}{[\Gamma^2 l^2 - \left(\frac{\Delta kl}{2}\right)^2]} \tag{8}$$

Where l is the length of the nonlinear material and Γ is the gain factor given by:

$$\Gamma^2 = \frac{8\pi^2 d_{eff}^2}{c\varepsilon_0 n_i n_s n_p \lambda_i \lambda_s} I_p \tag{9}$$

Where d_{eff} is the effective nonlinear coupling coefficient and I_p is the initial intensity of the pump field. A similar expression can also be derived for the fractional increase in idler field intensity. If we now assume that $\Gamma^2 l^2 << (\Delta k l/2)^2$, which is a reasonable simplification in most practical applications, the net single-pass small signal gain is established to be described by:

$$G_s(l) \cong \Gamma^2 l^2 [\frac{\sin\left(\frac{\Delta k l}{2}\right)}{\left(\frac{\Delta k l}{2}\right)}]^2 \tag{10}$$

The relationship between the single-pass small signal gain and the phase-mismatch parameter (or $\Delta k l/2$ to be precise) is shown graphically in Figure 1 and is the origin of the parametric gain bandwidth.

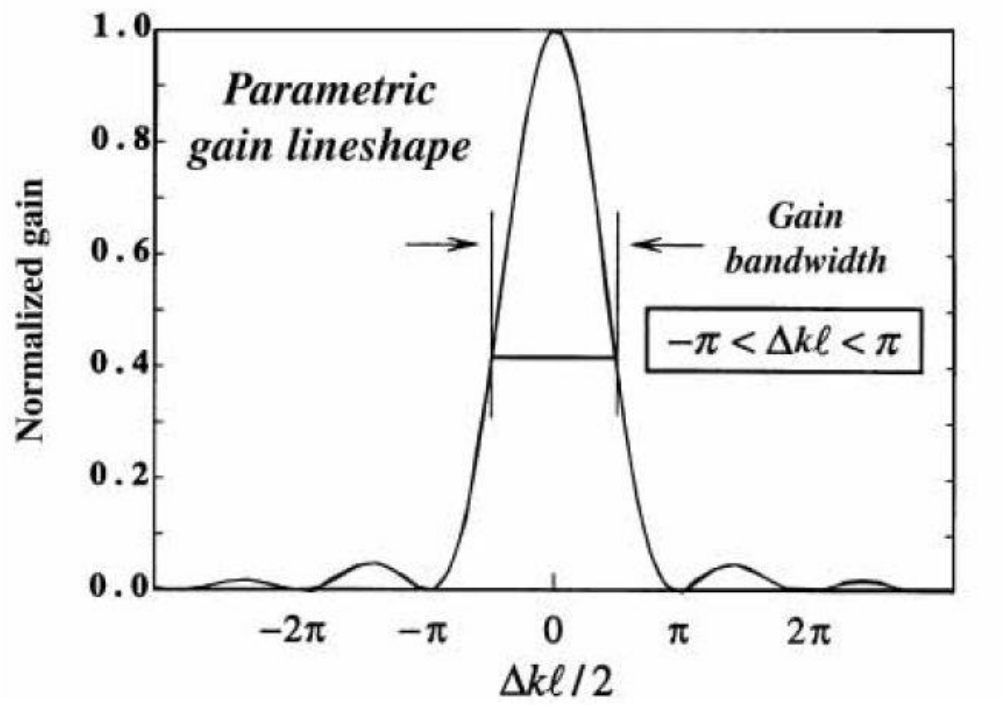

Figure 1: The relationship between gain and Δkl/2, showing the origin of the parametric gain bandwidth [27]

It is clear then that the phase-mismatch parameter is of profound importance in the efficacy of the parametric process, with both signal and idler field experiencing maximum amplification when $\Delta k = 0$. This is known as the phase-matching condition. However, since the pump, signal and idler field will each experience different refractive indices inside the nonlinear material, this condition cannot be satisfied off the bat. Thus phase-matching techniques must be employed, to engineer a situation where [25]

$$\omega_p n_p - \omega_s n_s - \omega_i n_i = 0 \tag{11}$$

in order to ensure maximum efficiency of the parametric process. The traditional approach is known as birefringent phase matching. Since nonlinear gain materials are usually anisotropic, the refractive index experienced by an incident optical field is dependent on propagation direction. Thus the orientation of the gain crystal determines which (if any) of the many possible signal and idler pairs satisfies the phase-matching condition and is able to oscillate. Unfortunately using this technique does not usually allow for all three optical fields to travel along the axis of maximum nonlinearity of the gain material, which results in less than optimal performance. A more recent approach, known as quasi-phase-matching, utilises so-called periodically poled materials, PPLN being one example, in which crystal domains are flipped periodically creating boundaries of periodic sign change in the nonlinearity of the material. When the propagating optical fields reach such a boundary, the phase shifts that have accumulated between them are reset. The fields can thus clear the entire length of the parametric gain medium with Δk remaining close to zero. In this case the signal and idler pair that is able to oscillate is determined by choosing an appropriate grating period length. While this length is dependent on temperature, thus facilitating temperature tuning of the device, a fanned grating design (shown in Figure 2) has also been a popular option, as it allows smooth tuning by simple lateral translation of the crystal. Figure 3 illustrates the difference between birefringent –and quasi-phase-matching in terms of down-converted field growth.

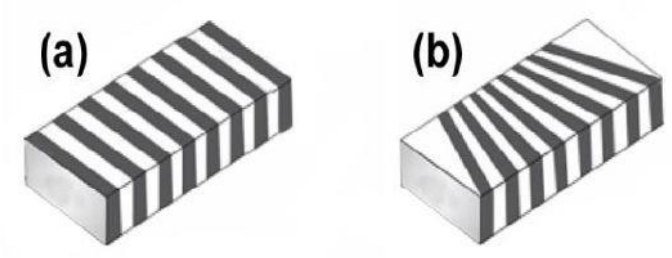

Figure 2: (a) A periodically poled crystal. (b) Such a crystal with a fanned grating design.

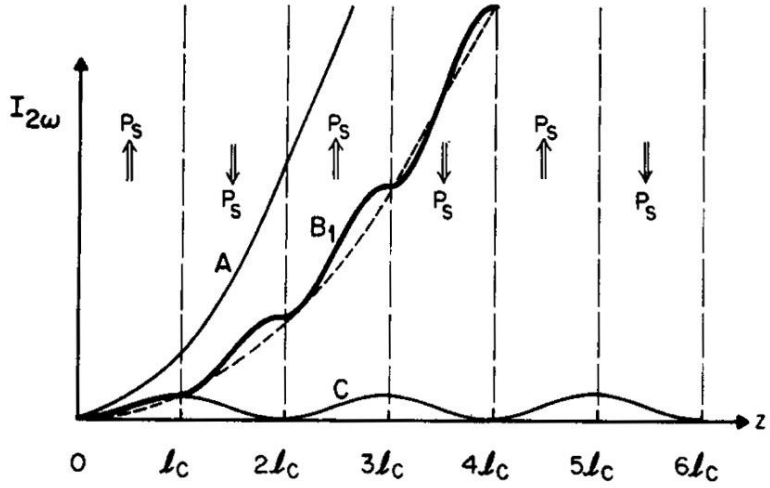

Figure 3: Down-converted field growth (in this case SHG) upon propagation through the nonlinear crystal, where c = coherence length. Curve A: Birefringent phase-matching, curve B_1: Quasi-phase-matching, curve C: no phase matching. [28]

2.1.3 The Singly-Resonant Intracavity OPO

In chapter one we saw that the SR ICOPO is by far the most ideal OPO cavity design for our purposes. Here we will discuss how to ensure maximum parametric performance within this configuration.

In any laser system, the level of output-coupling is an important factor in device performance, which will only be maximized when optimal output-coupling is employed. In a SR ICOPO the parent pump laser resonator consists of two HR coated mirrors and it is the OPO which is solely responsible for output coupling through down-conversion. It is thus of paramount importance to ensure that the OPO down-converts at a rate which simulates optimal output coupling of the laser if laser performance and OPO efficiency, in terms of primary pump power to idler output, are

to be maximized. The typical behaviour of an intracavity OPO system is shown in Figure 4.

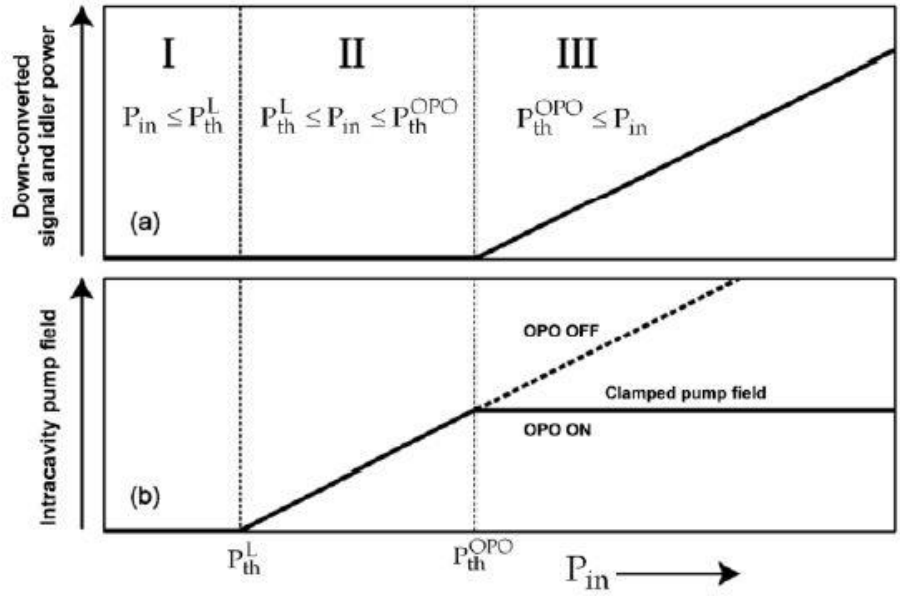

Figure 4: Typical operating behaviour of an intracavity OPO [29]

Once lasing threshold is reached, an initial linear build-up of pump field is observed, until the field intensity creates sufficient parametric gain in the nonlinear crystal to overcome cavity round-trip losses. The OPO is said to have reached threshold and parametric down-conversion begins. After this point, any increase in primary pump power promotes a linear response in signal and idler intensities, while the pump field is clamped at threshold value.

In order to achieve an optimised overall efficiency at a particular primary pumping level P_{in}, the following relationship between lasing and OPO threshold levels must be observed [17]:

$$P_{th}^{OPO} = \sqrt{P_{th}^{L} P_{in}} \tag{12}$$

where P_{th}^{OPO} is the OPO threshold level and P_{th}^{L} is the lasing threshold level, both thresholds being given in terms of primary pump power.

It is thus clear that manipulation of the OPO threshold level can be helpful in achieving an optimally functioning device. In terms of circulating pump field, this threshold level is governed by the following expression:

$$P_{th} = \varepsilon_0 c^3 \pi \frac{n_p n_s n_i (\varphi_p^2 + \varphi_s^2)}{4\omega_s \omega_i l^2 d_{eff}^2} \alpha_{cav} \tag{13}$$

where ϕ_p and ϕ_s are the waist radii of pump and signal beams inside the nonlinear crystal and α_{cav} is the round trip loss of the signal cavity. It can be seen that out of all the parameters the length l of the crystal and its nonlinear coefficient d_{eff} have the strongest impact on OPO threshold, which is why the development of materials such as PPLN, which facilitated the growth of far longer crystals, as well as possessing significantly higher nonlinear coefficients than previous materials, led to a substantial improvement in OPO technology. Once the nonlinear material is chosen, OPO threshold remains to be influenced by manipulation of the signal cavity round trip loss and the focusing of pump and signal beams inside the parametric crystal, the latter usually being the preferred option.

2.2 Spatial hole burning

In an ideal homogeneously broadened laser system all axial modes compete for the available optical gain within the active medium. The cavity mode closest to line-centre of the laser transitions' bandwidth reaches oscillation threshold first and is able to sweep out all of the gain, causing complete gain-saturation and leaving nothing for other potential modes. Such a system is thus characterised by single-frequency operation. However, in practice homogeneously broadened gain media, such as Nd:YAG, are known to sustain multiple spectral modes simultaneously, when operating within a standing wave cavity. In 1963 this behaviour was explained by Tang et al, who realized that it was due to a spatial modulation in the optical gain of the laser medium, caused by the electric field profile of the standing wave passing

through it [30]. A standing wave forms static regions of zero and maximum electric field, known as nodes and anti-nodes, which are separated by half a wavelength. When an optical wave of this form interacts with a pumped laser gain medium, stimulated emission will cause depletion of gain in regions of maximum-field, whilst gain in zero-field regions will be inaccessible and therefore left unsaturated. Rather than sweeping out the full optical gain stored in the pumped volume of the laser crystal, the standing wave 'burns holes' into the population inversion, resulting in an uneven spatial gain distribution as shown in Figure 5. A cavity mode whose anti-nodes coincide with the first mode's nodes, is then able to take advantage of the unsaturated gain and may itself reach lasing threshold. In this way, multiple cavity modes may oscillate simultaneously, despite the homogenously broadened nature of the laser transition. The effect can be minimized by placing the gain medium close to one end mirror of the laser cavity rather than centrally. As shown below, this increases frequency separation between spatially hole burnt modes, since a sufficiently large phase-shift between modes has to develop over a significantly smaller distance (see Figure 6).

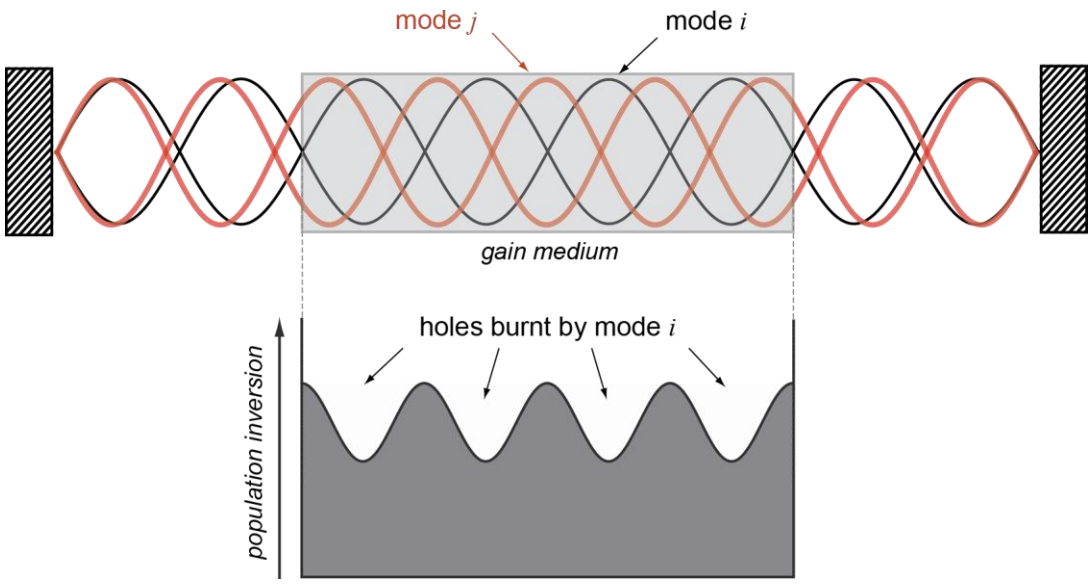

Figure 5: The effect of a standing wave pattern on population inversion inside the active medium and consequent multi-mode operation

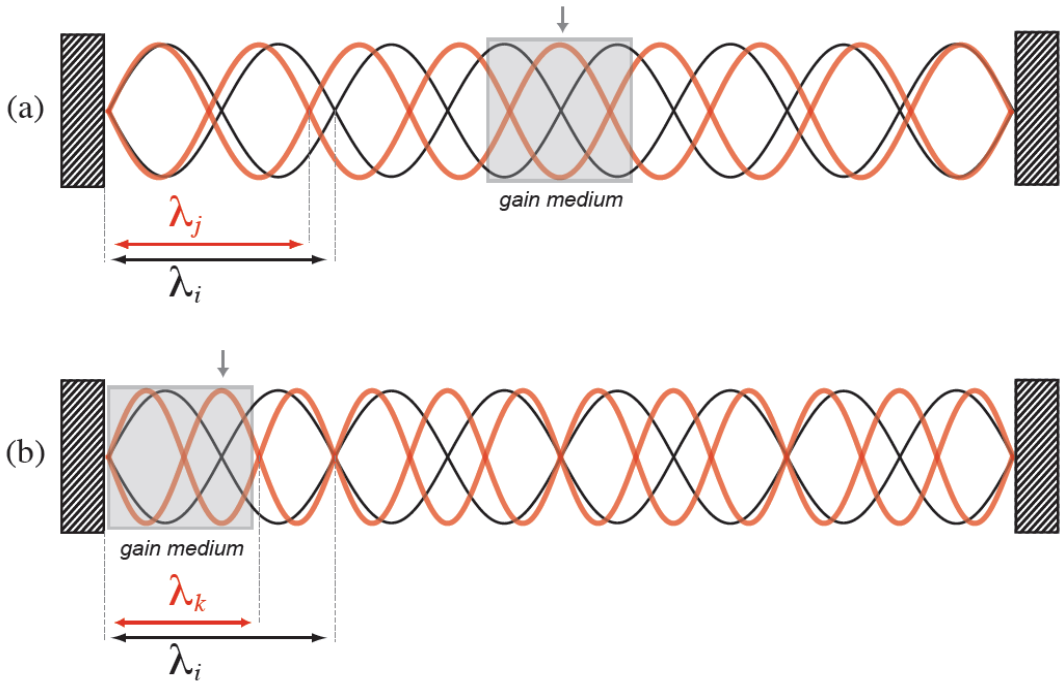

Figure 6: Illustrating why frequency spacing between spatially hole burnt modes is reduced by placing the laser gain medium close to one of the cavity end mirrors, rather than centrally

Consider a resonator of optical path length L with the centre of the gain medium (where the focus point of the pump beam is situated) a distance l away from the end mirror (Figure 7).

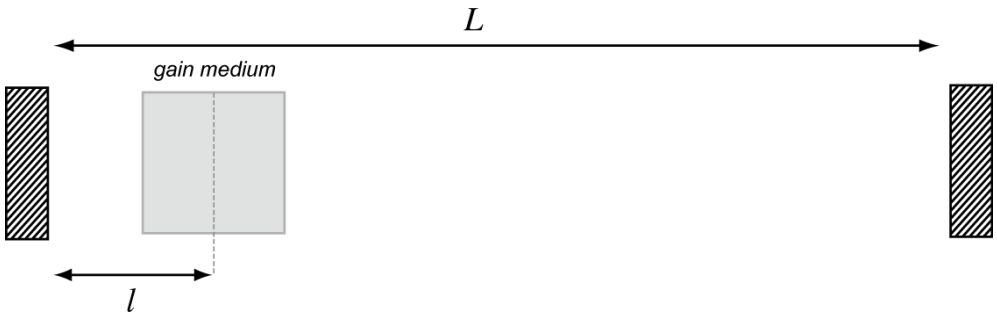

Figure 7: Schematic of a resonator cavity of length L with the centre of the gain medium a distance l away from the left hand mirror.

The frequency separation between adjacent cavity modes (known as the free spectral range) in such a system is given by:

$$\Delta\nu_{FSR} = \frac{c}{2L} \tag{14}$$

Take two possible cavity modes of wavelengths:

$$\lambda_1 = \frac{2L}{q_1} \tag{15}$$

and

$$\lambda_2 = \frac{2L}{q_2} \tag{16}$$

where q_1 and q_2 are respective mode numbers. In order for these two modes to oscillate simultaneously, one of them has to be given the opportunity to exploit the optical gain left behind by the standing wave pattern of the other. Thus, upon reaching the centre of the gain medium at distance l, a phase shift of $\pi/2$ has to have developed (as already illustrated in Figure 5). Given that all cavity modes have a node at the end mirrors of the cavity, the phase shift between the two modes at point l can be expressed as:

$$\Delta\phi = \frac{2\pi l}{\lambda_2} - \frac{2\pi l}{\lambda_1} \tag{17}$$

Setting this equal to $\pi/2$, to enable simultaneous oscillation, we get:

$$\frac{(\lambda_1 - \lambda_2)}{\lambda_1 \lambda_2} = \frac{1}{4l} \tag{18}$$

Making use of (15) and (16) this gives the axial mode separation between the spatially hole burnt modes:

$$q_2 - q_1 = \frac{L}{2l} \tag{19}$$

Since cavity modes are separated by the free spectral range given in (14), the frequency spacing can be found to be:

$$\Delta\nu = \frac{c}{4l} \tag{20}$$

It can thus be seen that placing the gain medium close to the end mirror of the cavity, as is in any case favourable in end-pumped solid state lasers, gives a greater frequency separation between spatially hole burnt modes, and therefore fewer oscillating modes, than placing the gain medium at the centre.

2.3 The Twisted-Mode Technique

This method aims to achieve single frequency operation by creating a uniform time-averaged optical intensity across the entire length of the laser gain medium, thus ensuring complete gain saturation and eliminating spatial hole burning. This is done by manipulating the polarization of light passing through the laser crystal.
Figure 8 shows the components and how they may be implemented in a diode pumped solid state laser.

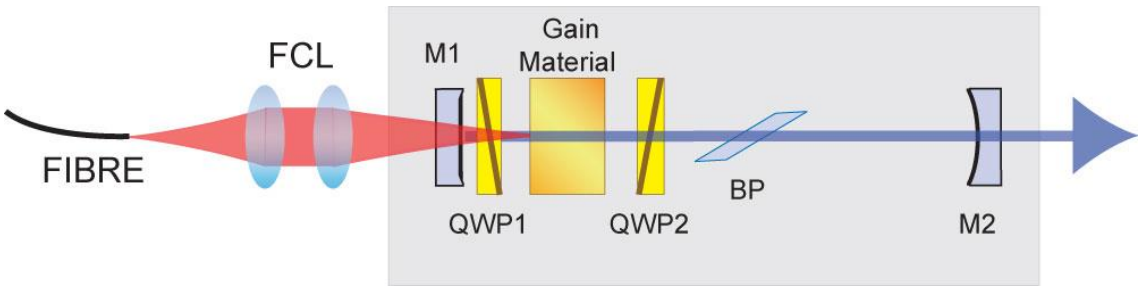

Figure 8: Cavity design including the twisted-mode components

A polariser such as a Brewster plate (BP) is used to select for a particular linear polarisation within the cavity. In component form this wave is described as follows [24]:

$$E_{x1} = E_{x0}\cos(kz - \omega t) \quad (21)$$

$$E_{y1} = E_{y0}\cos(kz - \omega t) \quad (22)$$

Where E_{x0} and E_{y0} are the magnitudes of the electric field vector in the x-direction (parallel to the optical bench and orthogonal to the laser beam) and the y-direction (orthogonal to both the optical bench and the laser beam), respectively.

This polarisation encounters quarter-wave plate 1 (QWP1) on its way to the gain medium and a $\pi/2$ phase shift between the x and y components is thus introduced:

$$E_{x2} = E_{x0}\cos(kz - \omega t - \frac{\pi}{2}) \quad (23)$$

$$E_{y2} = E_{y0}\cos(kz - \omega t) \quad (24)$$

This is the description of a wave which is left handed circularly polarised.

Quarter-wave plate 2 (QWP2) is placed at the other end of the crystal with its fast axis at 90 degrees to that of Q1 and thus counteracts the $\pi/2$ phase shift between x and y components, restoring original polarisation:

$$E_{x3} = E_{x0}\cos\,(kz - \omega t - \frac{\pi}{2}) \quad (25)$$

$$E_{y3} = E_{y0}\cos(kz - \omega t - \frac{\pi}{2}) \quad (26)$$

This wave is reflected off the end mirror and now travelling in the opposite direction, makes a further pass through Q2 before entering the gain medium for the second time:

$$E_{x4} = E_{x0}\cos[kz + \left(\omega t - \frac{\pi}{2}\right)] \quad (27)$$

$$E_{y4} = E_{y0}\cos[kz + (\omega t - \pi)] \quad (28)$$

This describes a right handed circularly polarised wave. Finally, a second pass through Q1 once again restores original linear polarisation and completes the round trip.

Figure 9 shows regions 1, 2, 3 and 4 of the laser cavity for reference.

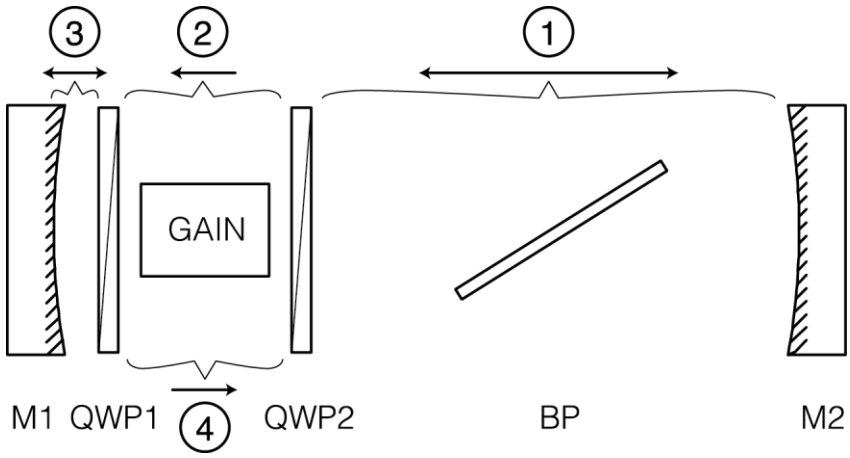

Figure 9: The various laser cavity regions used in the above analysis.

Let us now consider the superposition of the two counter-propagating waves inside the gain medium:

$$E_{xgain} = E_{x2} + E_{x4} = 2E_{x0}\sin(kz)\cos(\omega t) \tag{29}$$

$$E_{ygain} = E_{y2} + E_{y4} = 2E_{y0}\cos(kz)\cos(\omega t) \tag{30}$$

The resultant optical intensity is given by:

$$I \propto E_{xgain}^2 + E_{ygain}^2 = \left(2E_{x0}^2 + 2E_{y0}^2\right)\cos^2(\omega t) \tag{31}$$

It can be seen from this result that the optical intensity inside the laser gain medium is *not* dependent on position and can thus be said to be spatially uniform. The optical gain stored in the active medium will be swept out in its entirety, prohibiting spatial hole burning and resulting in single frequency operation.

In this chapter we have familiarised ourselves with the underlying physical concepts of parametric generation, the origin of multi-mode behaviour in homogeneously broadened laser systems and the twisted-mode technique as a way of achieving a

single frequency source, the practical application of which will be the subject of chapter three.

Chapter Three: The Basic Laser

This chapter describes the design and performance of the basic 1μm pump laser and evaluates the efficacy of the twisted-mode approach in this context.

3.1 Basic Laser Design and Characterisation

3.1.1 The Pump Head

Given that this investigation was to be centred around an end-pumped Nd:YAG based laser system, a 10W 808 nm fibre-coupled (200 μm fibre diameter), temperature-stabilised laser diode was the natural pump source choice (Axcel Photonics, part number: HF-808-010W-250). The temperature of the diode was varied as a function of its pumping current to ensure its emission wavelength coincided with the peak absorption wavelength of Nd:YAG at 808 nm. The pump light was passed through two plano-convex spherical focusing lenses, AR coated for pump wavelengths and with a focal length of 50 mm each, resulting in a pumped-volume radius of 110 μm in the laser gain medium, as seen in Figure 1.

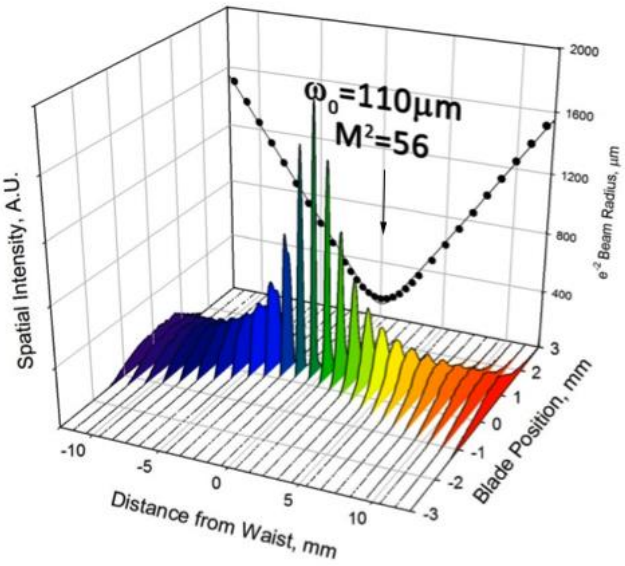

Figure 1: Diode pump beam profile. This measurement was obtained using the moving blade technique as described below (see thermal lens measurement).

As shown in Figure 2 the diode came to threshold at a pumping current of 2 A and exhibited a slope efficiency of 0.995 W/A. Using an OSA the diode wavelength was carefully monitored during this measurement and the temperature set-point adjusted and recorded at each pumping level, keeping the wavelength at 808 nm, which would be important to ensure the efficient pumping of the laser gain crystal later on. For our purposes a power output of 3-4 W was sufficient, as higher pumping levels might have caused laser crystal damage.

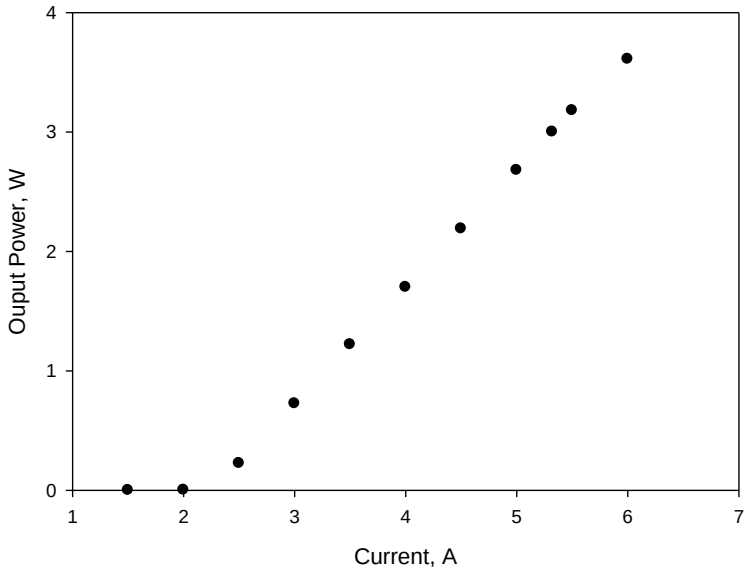

Figure 2: Diode power characterisation, measured using a high-power thermal power meter. The device came to threshold at 2 A and exhibited a slope efficiency of 0.995 W/A.

3.1.2 Cavity Design

A simple Nd:YAG laser was first constructed in order to test the efficacy of the twisted mode approach for the suppression of spatially hole burnt modes in a familiar system. Legacy components from Nigel Gallaher's project were used for this purpose, including a 5λ/4 quarter-wave plate, AR coated for pump wavelengths and HR coated for 1064 nm on one side, which served as a cavity end mirror and back quarter wave plate simultaneously, a 5x3 mm cylindrical Nd:YAG crystal, both facets of which were AR coated at 1064 nm and a further 5λ/4 quarter-wave plate, AR coated at 1064 nm on both sides [24]. Low order wave plates are highly desirable for our purposes as they exhibit less sensitivity to wavelength and temperature variance. These components

were mounted using three hollow brass cylinders, which were engineered to a sliding fit into one another, as shown in Figure 3 and 4. This allowed each component to be rotated individually.

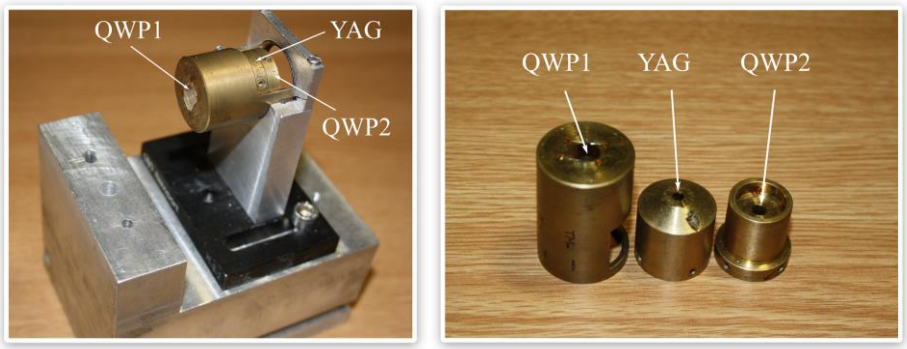

Figure 3: Twisted-mode components in their mounts

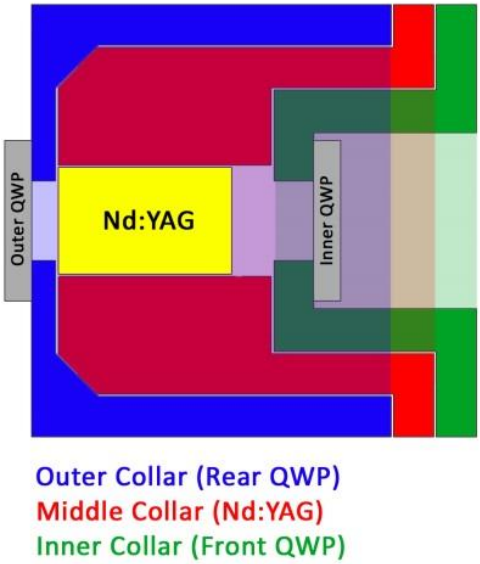

Figure 4: Detailed schematic of brass collar design for mounting twisted-mode components

A basic cavity was first designed using only the back quarter wave plate, the Nd:YAG crystal and a 90% plane output coupler, which was positioned appropriately to ensure a good match between pumped volume and circulating field inside the gain material. The resultant laser yielded 995mW of 1μm output for 3W of diode pump power. The thermal lens induced in the active medium (an important cavity design parameter) was evaluated by taking beam profiles at various distances from the output coupler and using the Gaussian beam propagation equations [31]:

$$\omega_z = \omega_0 \sqrt{[1 + \left(\frac{z\lambda}{\pi\omega_0^2}\right)^2]} \quad (1)$$

$$R = z[1 + \left(\frac{\omega_0^2 k}{2z}\right)^2] \quad (2)$$

where ω_z is the beam radius at a distance z from the beam waist, ω_0 is the beam waist size, λ is the wavelength of the laser and R is the thermally induced radius in the gain medium. This approach depends on accurate knowledge of beam waist position, assured through the use of a plane output coupler. Having calculated ω_0 and knowing the cavity length L, the thermally induced radius of curvature exhibited by the Nd:YAG can be deduced. The experimental set-up employed is shown schematically in Figure 5a, while results of this measurement can be found in Figure 5b.

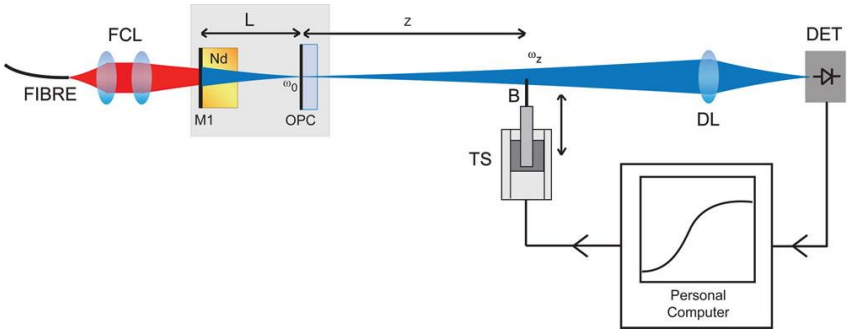

Figure 5a: Experimental set-up for thermal lens measurement

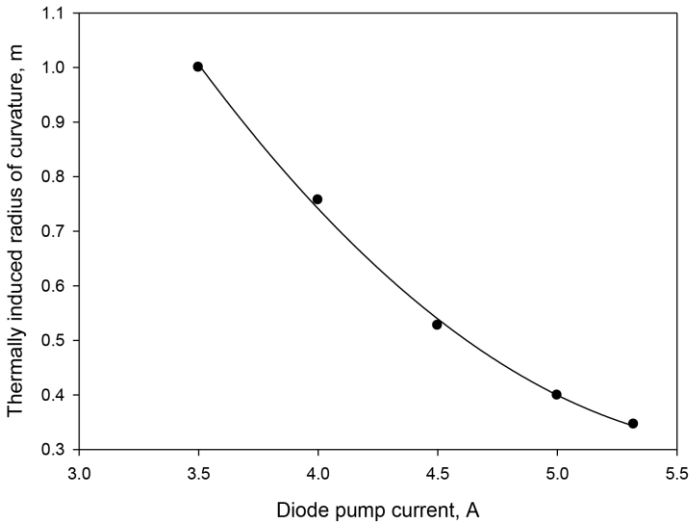

Figure 5b: Thermal lens in the Nd:YAG gain material. The radius of curvature given here represents that of the mirror needed to create an equivalent cavity in the absence of thermal effects.

At a pumping level of 3W (93% of which was absorbed by the gain material), our chosen operating point for future investigations, a thermal lens of focal length 35cm was observed.

3.2 The Twisted Mode Technique Applied to the Basic Laser

3.2.1 Alignment of the Quarter-Wave Plates

The twisted mode approach requires two quarter wave plates either side of the gain medium, with their fast axes at 45 degrees to the optical axis of the laser and at 90 degrees to each other. The correct rotational positions of the plates were established using the set-up shown in Figure 6.

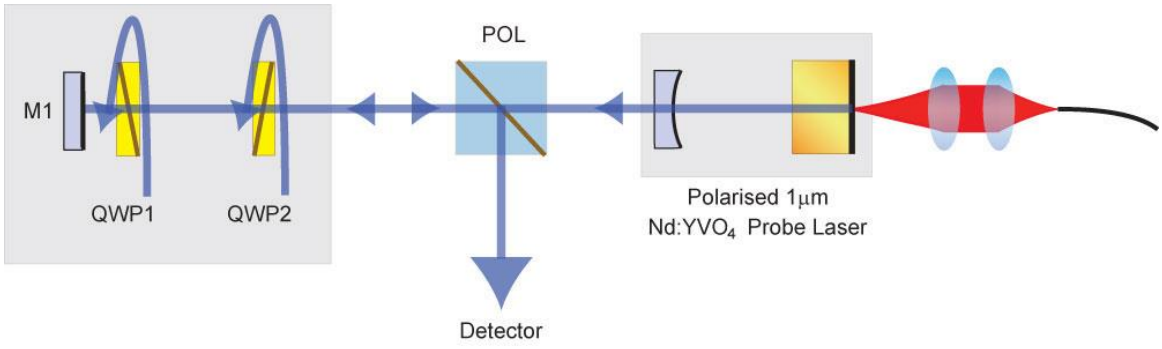

Figure 6: Quarter-wave plate alignment set-up.

A probe laser was built based on Nd:YVO_4, an anisotropic gain medium, which yields 1μm light of a known linear polarisation. The orientation of the crystal was chosen such that the output was horizontally polarised. The beam of the probe laser was guided through a polarising beam cube and onto the back quarter-wave plate of the Nd:YAG system. Due to the 1μm HR coating on the outside surface, the light was reflected after passing through the plate and made its way back to the polarising beam cube. By monitoring the rejection level of this beam cube, the polarisation of the incoming light could be determined. Since a double pass through a quarter-wave plate was experienced, the polarisation of the light should now have been vertical and beam cube rejection should be maximised if the plate's orientation was correct. After

determining both the 'active' and 'neutral' positions of the first plate, the second quarter-wave plate was inserted between the first plate and the beam cube. Since the light was now experiencing four quarter-wave plate passes on a round trip (i.e. a full wave of retardation), its polarisation should have been returned to the original state upon reaching the beam cube, minimising rejection. Once again both the 'active' and 'neutral' orientations of the second quarter-wave plate were found in this manner. The oscilloscope traces in Figure 7 were taken with the help of a rotating beam cube and serve to better visualise this alignment process.

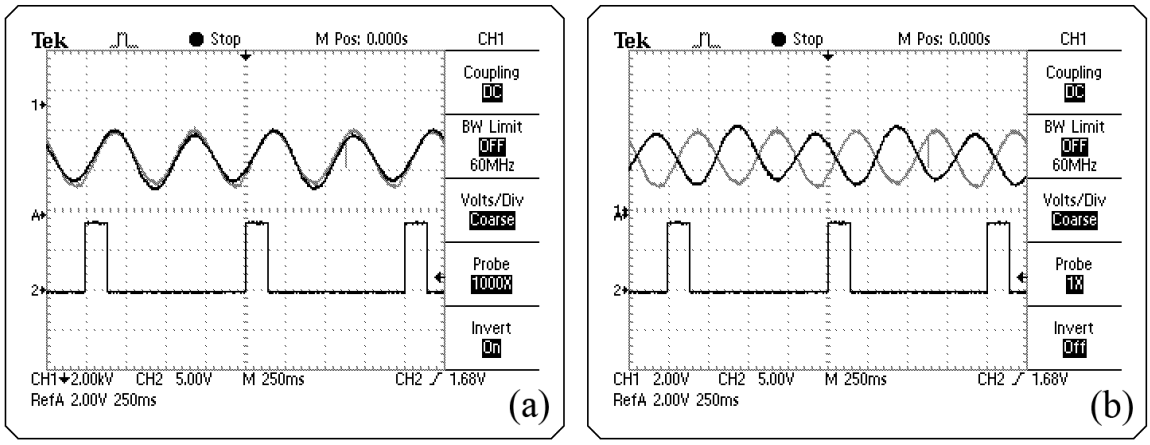

Figure 7: A rotating beam cube set-up allowed us to view shifts in polarisation due to rotation of the quarter-wave plates in real time. The grey trace is a reference trace, while the black trace was shifting as quarter-wave plates were rotated. (a) The light experienced no polarisation change after passing through the plates. (b) The plates caused a shift from horizontal to vertical polarisation.

3.2.2 Construction and Characterisation of the Twisted-Mode Laser

Next the twisted mode components were incorporated into the pump laser. In order to accommodate a further quarter wave plate and a Brewster plate, the laser cavity described in the previous section was extended by replacing the plane back mirror with a 200mm radius of curvature output coupler of the same reflectivity. The new cavity design is shown in Figure 8. As expected, similar output powers were achieved. An unexpectedly high drop in power of 30.7% was observed upon insertion of the second quarter wave plate in both the active and neutral orientations, which was put down to a reduction in the optical quality of the plate due to age, as well as

manoeuvrability constraints imposed by the mounting system. The decision was therefore made to replace this quarter wave plate with a new zero-order plate, which resulted in a far lower power penalty of just 6.4%. We realised that replacing the back quarter wave plate was likely to have a similarly positive impact on our system's performance, especially since close inspection revealed a very fine fracture at the centre of the plate. This was however a more complicated undertaking, given that the back quarter wave plate was also acting as a cavity end mirror, and an equivalent component was not available to us. We therefore opted for a separate plane end mirror, AR coated for pump wavelengths on both sides and with a 1μm HR coating on the intracavity surface, in conjunction with a new zero order quarter wave plate, which was AR coated at 1μm on both sides. Because this plate was not AR coated for pump wavelengths, a drop in pump power of 37% had to be compensated for by increasing pump current, in order to maintain the pumping level of the laser gain medium. Furthermore, the space between the pump head and the pump beam focus at the centre of the gain medium was found to be insufficient to accommodate the new set-up and longer focal length lenses (75mm) had to be used in the pump head to focus the pump beam more gradually over a longer distance. However, the rewards reaped in terms of system performance were indeed significant in; 1.236W (compared to a previous 995mW) of output for 3W of incident diode pump were able to be extracted. This dropped to 1.079W with insertion of the (new) second quarter wave plate.

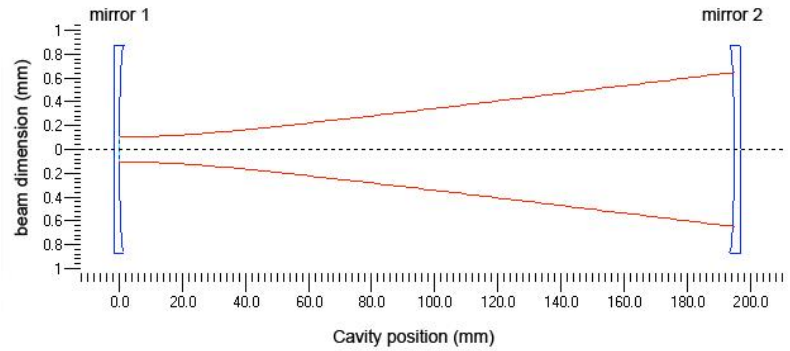

Figure 8: Extended cavity design, created in PSST! Mirror 1 has a radius of curvature of 3500 mm (representing the thermal lens induced in the gain crystal), and mirror 2 has a radius of curvature of 200 mm. The operation wavelength is 1064 nm.

After repeating the quarter wave plate alignment procedure, the Brewster plate, set to select for horizontal polarisation, was next to be included, however the resultant insertion loss was found to be unusually high with significant rejection off the plate, which we felt required further investigation. The Nd:YAG crystal was checked for birefringence, which, if present, would cause additional rotation of the circulating field's polarisation, preventing restoration of original polarisation over a round trip and therefore leading to loss at the Brewster plate as well as elliptical rather than circular polarisation inside the active medium, leading to non-homogeneous gain saturation and therefore spatial hole burning. The result is shown in Figure 9a. It can clearly be seen that the grub screw, which held the crystal in place, was indeed causing stress-induced birefringence and an alternative mounting method (Figure 9b) had to be employed to eliminate the problem. Now the Brewster plate was found to have a much improved power drop of just 1.5%. With all components in place the laser came to threshold at 0.82W of diode pump power and an output power of 1.063W for 3W of diode pump was achieved. A full power characterisation of the system can be found in Figure 10.

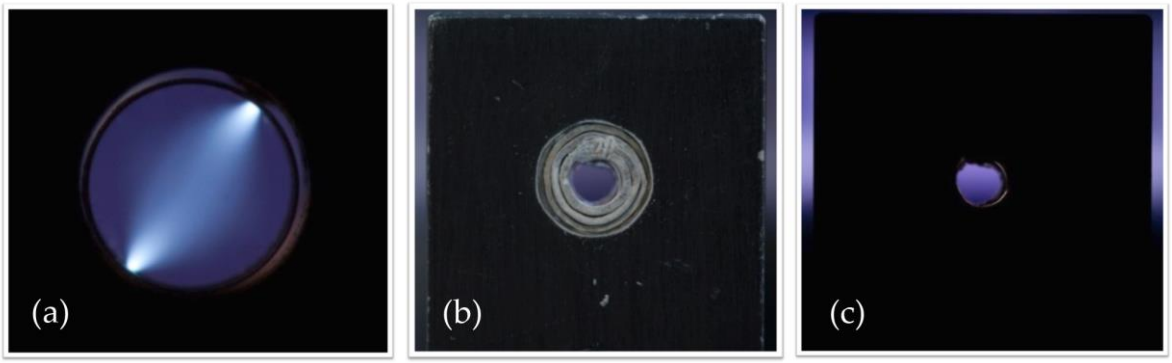

Figure 9: Birefringence in the gain medium. These pictures were produced by placing the Nd:YAG between two crossed polarisers with a flash gun on one side and a camera on the other.(a) The light area indicates stress-induced birefringence caused by a grub screw clamping down on the Nd:YAG crystal. (b) To eliminate the problem a new mount was constructed in which the crystal was wrapped in indium foil and pressed into a tapered hole to keep it in place. (c) No birefringence is observed in the new mount.

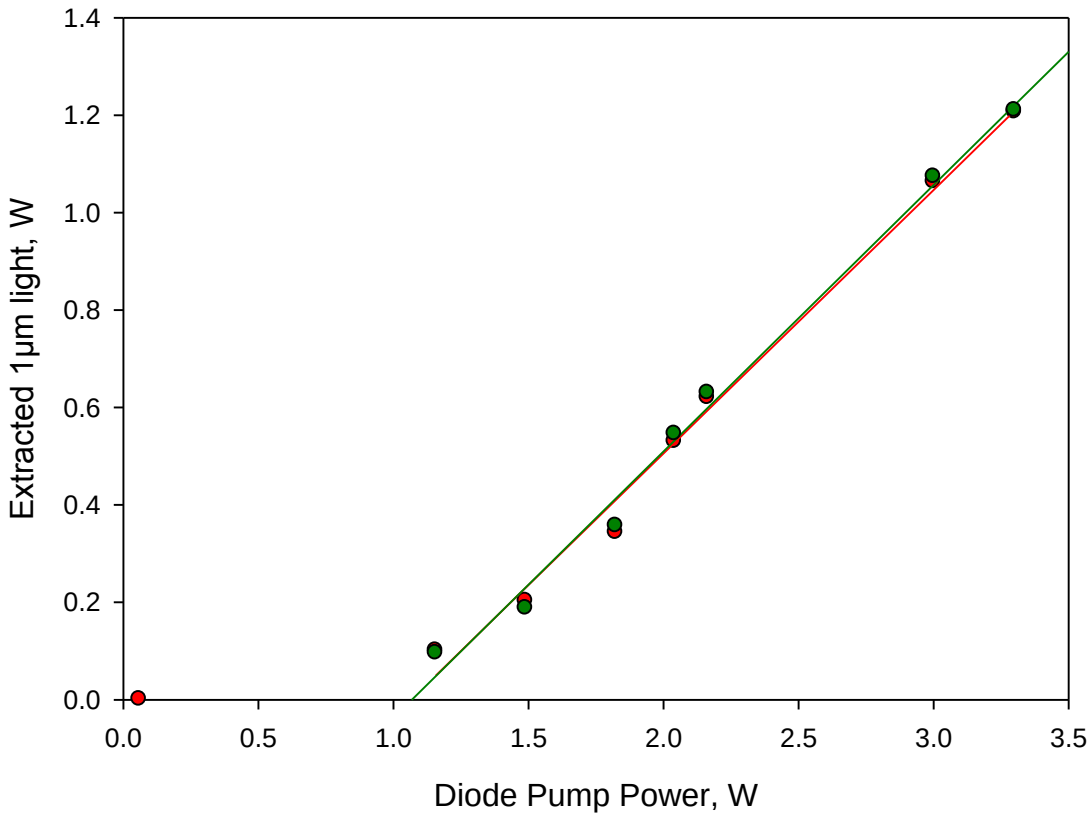

Figure 10: Power characterisation of the basic laser with quarter-wave plates in the 'active' position (red) and 'neutral' position (green).

A photograph of the completed basic laser is shown in Figure 11.

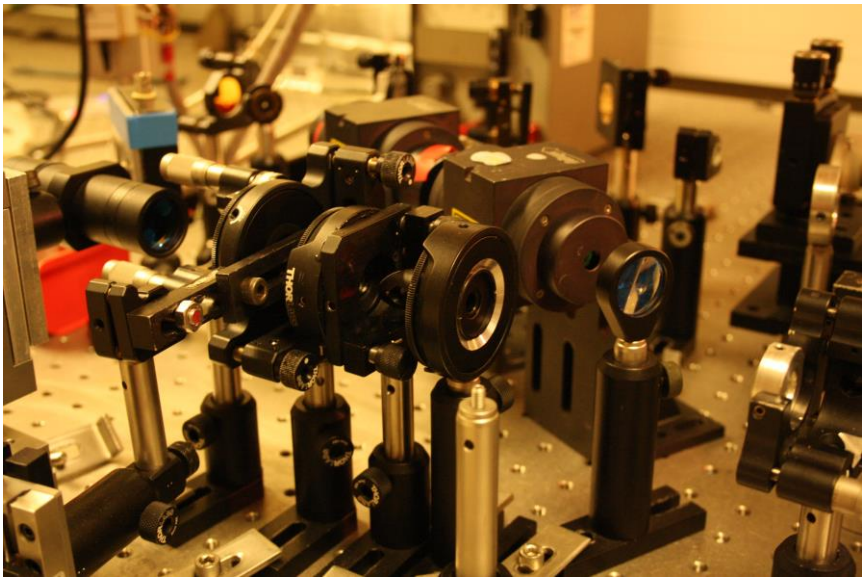

Figure 11: The Twisted-Mode Technique implemented in a basic 1 µm laser

3.2.3 Impact of the Twisted-Mode Technique on Frequency Behaviour

It was now time to assess the efficacy of the twisted-mode technique in the elimination of spatial hole burning. A 200 GHz free spectral range (0.75 mm separation) home built plane-plane scanning Fabry-Perot interferometer was used to monitor the coarse mode structure of our laser's frequency spectrum, which would reveal the presence or absence of spatial hole burning, while a commercial scanning confocal interferometer with a 2 GHz (7.5 cm separation) free spectral range (Tec-Optics) allowed us to simultaneously investigate mode fine structure, thus offering a complete picture of frequency behaviour. Isolators were used to eliminate the frequency-stability-disturbing effects of back-reflection into the laser. A single isolator proved insufficient in this situation and a second isolator had to be employed to fully prevent back-reflection and the erratic multi-mode behaviour associated with it, due to the fact that single-frequency lasers are very sensitive to such disturbance.

In order to establish a frequency behaviour base line, both quarter wave plates were first turned to a neutral orientation, creating a standard Nd:YAG laser in the usual standing wave configuration. The coarse frequency spectrum of this laser is shown in Figure 12. This oscilloscope trace clearly shows 4-6 modes oscillating simultaneously. From expression (20) in chapter two we would expect a frequency separation of ~25 GHz between spatially hole burnt modes. The observed separation, at ~20 GHz, is in reasonable agreement with this estimate.

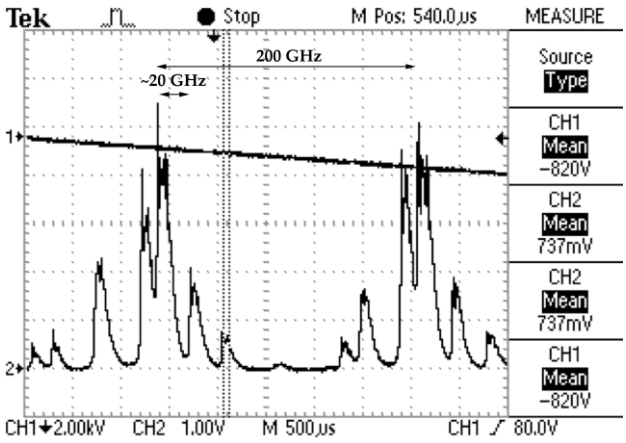

Figure 12: Without the twisted mode effect spatial hole burning is causing multi-mode behaviour. This trace was taken with our 200 GHz scanning plane-plane interferometer and thus gives a comprehensive overview of the entire laser gain bandwidth.

Next both quarter wave plates were rotated to their active positions, thus initiating the twisted-mode effect. The resultant frequency behaviour is shown in Figure 13. The laser was now operating on a single longitudinal mode for minutes at a time and always settling back down to this behaviour after mechanical disturbance. It is clear that the twisted-mode technique did indeed prove very effective in the elimination of spatial hole burning.

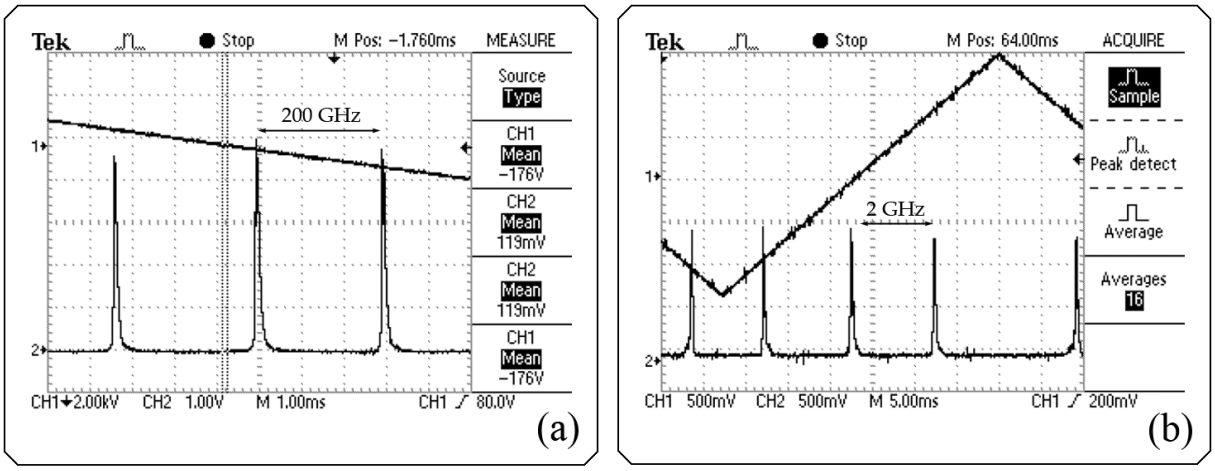

Figure 13: The successful elimination of spatial hole burning is evident. Trace (a) was taken with our 200 GHz scanning plane-plane interferometer. Since any spatially hole burnt modes would have been expected to lie ~20 GHz from the primary mode, they would have been easily resolved by the interferometer. Trace (b) was taken with our 2 GHz scanning confocal interferometer. Since the mode spacing in this system was ~750 MHz, the next cavity mode would once again have been easily resolved. Both interferometers thus indicate single-frequency operation.

In this chapter the construction and characterisation of a simple Nd:YAG laser was described. The twisted-mode approach was assessed in this context and was found to be an effective means of ensuring single frequency operation. The next chapter will describe the inclusion of the intracavity OPO and its effects on frequency behaviour of the pump laser. Will the twisted-mode technique still be successful in eliminating multi-mode operation?

Chapter Four: The OPO

In this chapter we will use the Nd:YAG laser described in chapter three to pump a PPLN based intracavity OPO. After carrying out a basic characterisation of this system, the twisted-mode technique will once again be applied and its efficacy in enabling single frequency operation of the pump field assessed.

4.1 OPO Design and Characterisation

4.1.1 The extended laser cavity

In order to accommodate the OPO components, the cavity of the basic 1μm laser was extended initially to 485cm, utilizing a 90% reflective, 200mm radius of curvature output coupler as well as a 60mm focal length lens to ensure cavity stability and, later on, suitable focusing in the nonlinear crystal. Whilst a cavity of this length provides less than ideal conditions for achieving stable single frequency operation (due to the reduction in frequency space between adjacent cavity modes), we were at this point limited by the radius of curvature of the output couplers available to us. Figure 1 shows the extended pump laser cavity design. Once again good overlap between the pumped and circulating field volumes inside the Nd:YAG was a design priority. No noticeable drop in power was observed compared to the previous configuration (indicating the intracavity lens to be a very low loss component).

For reasons already discussed in chapter one, a singly resonant intracavity design, in which the signal field is resonated and the idler exits after a single pass, was deemed the most suitable configuration for our purposes as it releases the cavity from the stability restraints of the doubly-resonant condition. The traditional SRO ICOPO design is shown in Figure 2.

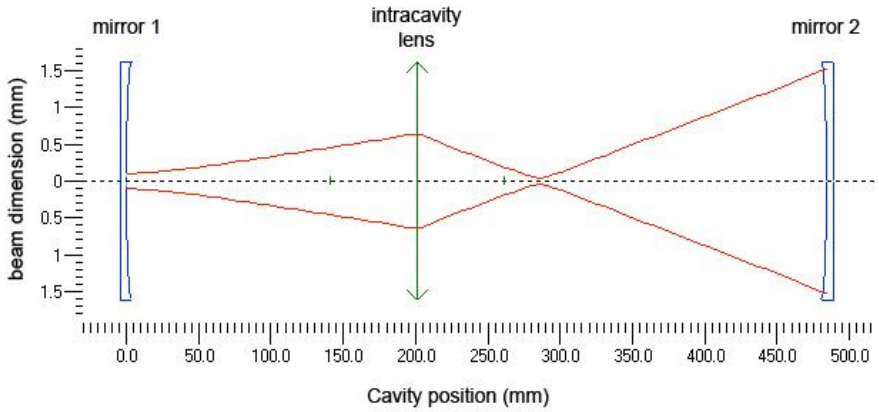

Figure 1: Extended 1µm laser cavity design created in PSST! at an operation wavelength of 1064 nm. Mirrors 1 and 2 have a radius of curvature of 3500 mm and 200 mm respectively. The intracavity lens has a focal length of 60 mm. The

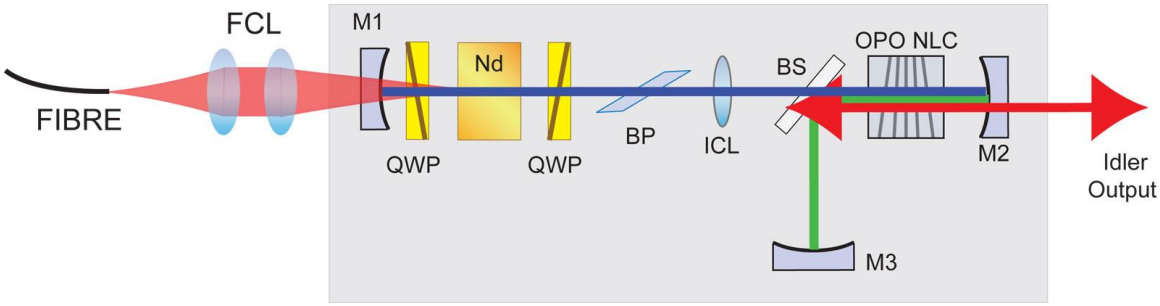

Figure 2: Schematic of the twisted-mode technique implemented in a traditional singly-resonant intracavity OPO design.

Here the signal cavity is defined by the pump cavity end mirror (M2), which is HR coated at both pump and signal wavelengths, a dichroic beam splitter BS, to be placed in-between the intracavity lens and the nonlinear crystal at an angle of 10° to the laser beam and a further end-mirror external to the pump cavity (M3). Upon insertion of the beam splitter, which was AR coated at pump wavelengths on both sides and HR coated for signal wavelengths on the side facing the nonlinear crystal, a power drop of 13.8% (from 1.08W to 0.931W) was observed. The 30x8x1mm^3 PPLN crystal had both facets AR coated at pump, signal and idler wavelengths and featured a fanned grating design, as described in chapter one, with grating periods ranging from 29.5µm to 32.5µm. It was mounted on a lateral translation stage, enabling coarse tuning of signal and idler wavelengths. If our system was to be used as a spectroscopic source, the

temperature of the PPLN crystal would have to be carefully stabilised, since absolute idler frequency and its stability would be important. However, since spectroscopic applications were beyond the scope of this project we chose not to do so at this stage. Because $LiNbO_3$ is a birefringent material, it was important to ensure that the fast axis of the crystal was accurately aligned to match the linear polarisation of the circulating field of the laser in order to prevent polarisation perturbations, which would result in elliptical rather than circular polarization in the laser gain material and thus spatial hole burning. The crystal was therefore mounted on a goniometer-type adjustable mount, facilitating rotation of the PPLN around the axis of the laser beam and orthogonal to it in both possible senses, as well as lateral translation. The insertion of the nonlinear crystal into the 1μm laser cavity resulted in a power drop of 0.9%. Frequency behaviour was re-assessed at this point before proceeding, to ensure spectral stability had not been affected. Fortunately, single frequency operation was once again observed when the twisted-mode technique was applied, indicating correct PPLN alignment. It was also found that misalignment of the crystal could indeed induce multi-mode behaviour as expected. With the pump cavity now fully equipped for OPO operation, the optimum output coupling level, which would later be used to assess OPO down-conversion efficiency, was measured and found to lie at 10%, with 0.923W of 1μm light being extracted for 3W of diode pump power (Figure 3).

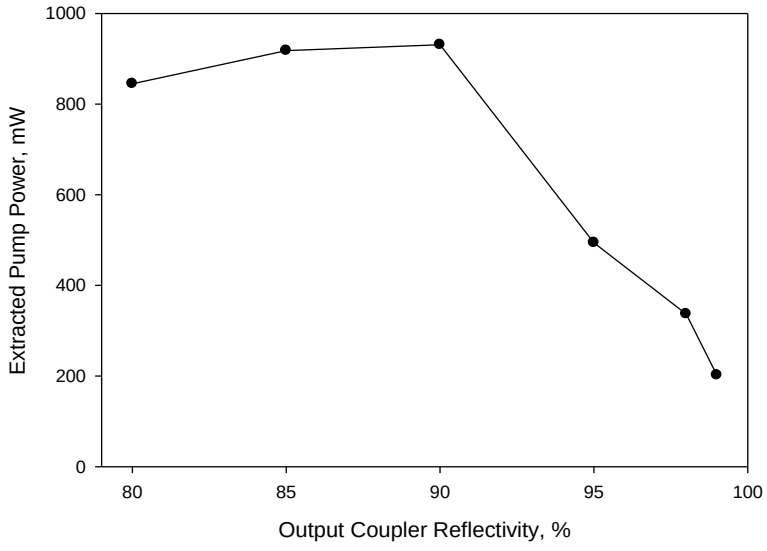

Figure 3: Optimum output coupling results for the extended pump cavity

A power characterisation of the system is shown in Figure 4.

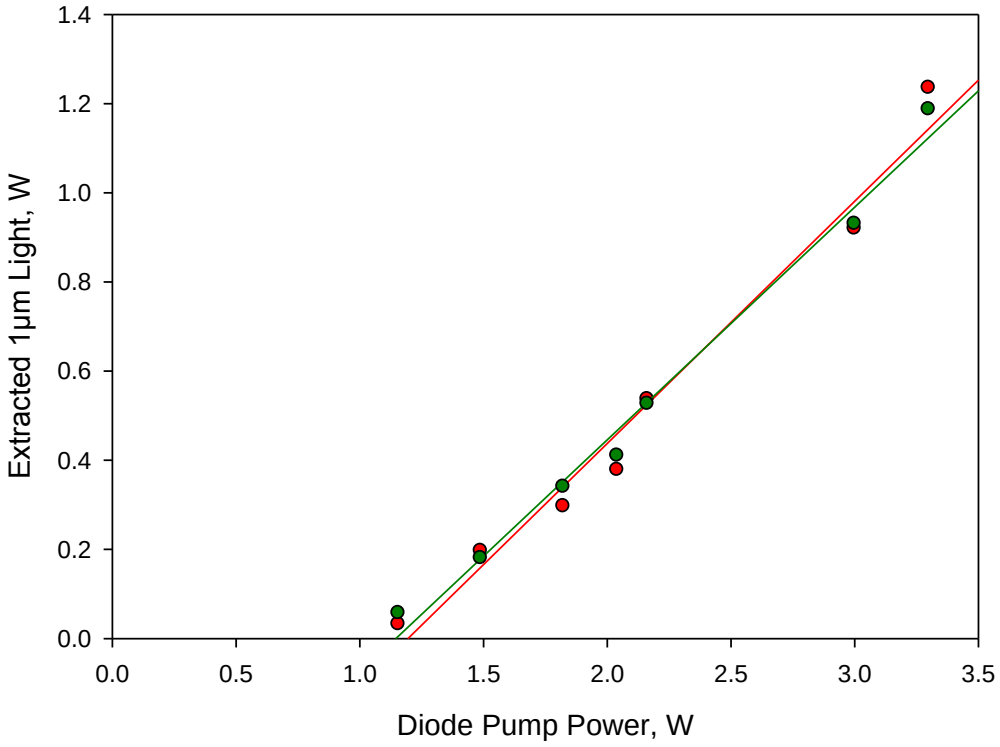

Figure 4: Power characterisation of the pump laser cavity including OPO components with quarter-wave plates in the 'active' position (red) and quarter-wave plates in the 'neutral' position (green.

With characterisation of the extended laser cavity complete, the 200mm radius of curvature output coupler was replaced with a 30mm radius of curvature high reflector for pump and signal wavelengths, and the cavity length adjusted accordingly (Figure 5), in preparation for OPO operation. The use of a significantly shorter focal length mirror has the dual benefit of increasing the free spectral range of the laser (from ~300 MHz to ~450 MHz) and also making it more geometrically stable, particularly in the face of thermal effects induced within the PPLN crystal. In this configuration laser threshold was measured to lie at 0.07W of diode pump. Thus to maximise idler output at a pumping level of 3W, our OPO threshold needed to lie at 0.458W according to expression (12) in chapter two.

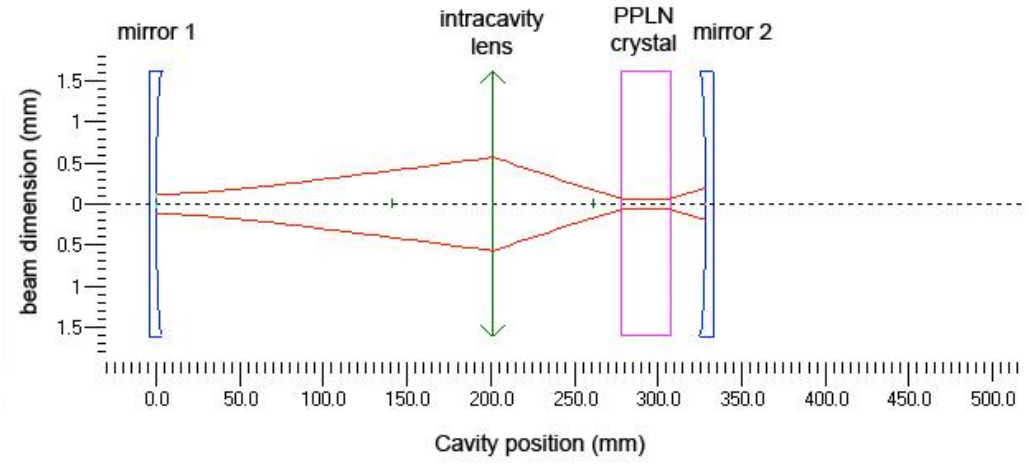

Figure 5: OPO 1μm pump cavity design created in PSST!

4.1.2 The OPO

Finally, to facilitate OPO operation a 50 mm radius of curvature mirror was placed at the outboard end of the signal cavity, such that signal and pump volumes would overlap well inside the nonlinear crystal, thus maximising parametric interaction between the two fields. The signal cavity design is outlined in Figure 6, while Figure 7 shows the mode-overlap between pump and signal fields inside the PPLN crystal.

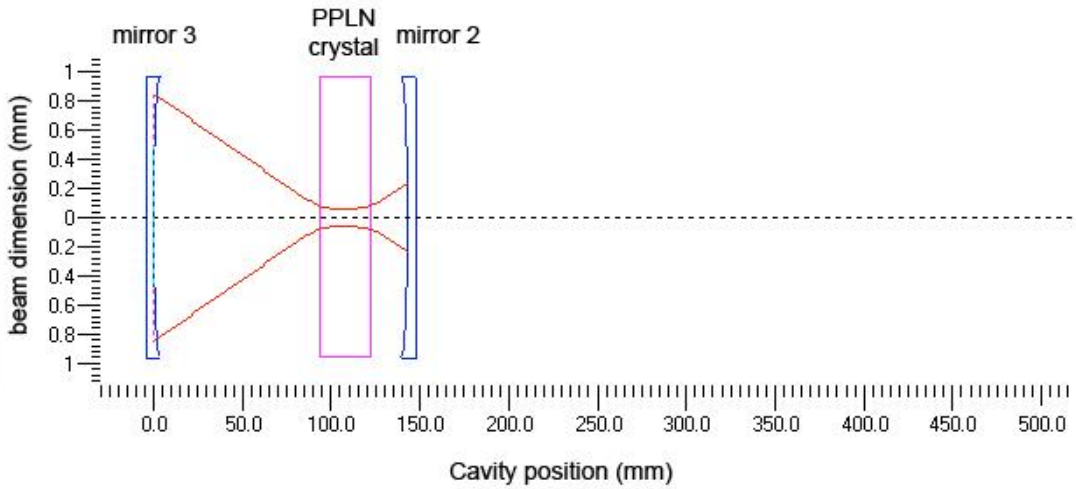

Figure 6: Signal cavity design created in PSST!. Here mirror 2 is a common end-mirror shared with the pump cavity (ROC=30 mm), while mirror 3 is placed at the outboard end of the signal cavity (ROC=50 mm). The operation wavelength is 1600 nm.

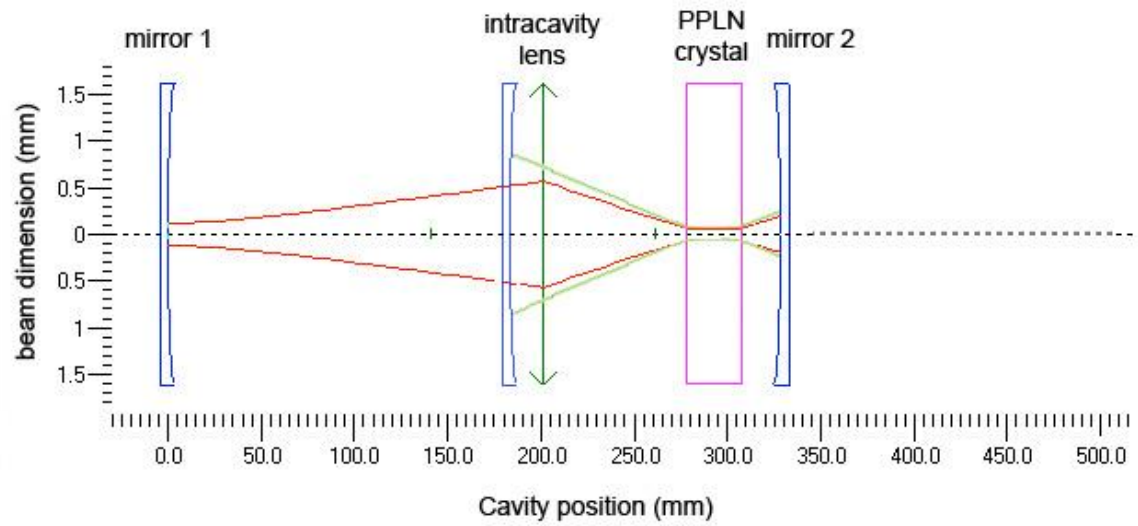

Figure 7: A superposition of pump and signal cavities, showing the mode-overlap between pump (red line) and signal (green line) fields inside the nonlinear medium.

However, since the end-mirror happened to be HR coated at both signal and pump wavelengths, double-passed pump light would be able to re-enter the pump cavity, which has been shown to drastically exacerbate the problem of relaxation oscillations, and in turn cause frequency instabilities. Therefore a second beam splitter placed between the original beam splitter and the outboard signal mirror, as shown in Figure 8, was deemed an appropriate design modification for our purposes, since it would significantly reduce these coupled-cavity effects by effectively reducing the fed back pump by a factor of 10^4 (assuming a ~1% reflectivity at pump wavelengths). The finite loss of the beam splitters at both pump and signal wavelengths was exploited in order to accommodate the various diagnostic instruments required to measure circulating field strength, frequency structure, etc. A photograph of this design is shown in Figure 9. With both the pump and signal cavities complete and quarter wave plates in the 'active' position, the OPO came to threshold at a diode pump power of 1.157W (corresponding to a circulating field power of 5.61W). This value is considerably higher than the ideal threshold calculated above (0.458W of diode pump). A similar result was also obtained when quarter wave plates were turned to the 'neutral' position, indicating that the twisted-mode technique was not the cause of the extra loss. Using

equation (13) from chapter 2 we can deduce the signal cavity round-trip loss to be 2.7%. Using the same equation we can work out that the optimum OPO threshold of 0.458W of diode pump power (corresponding to 1.2W of circulating pump field) would require pump and signal focal radii of 37.3 μm (rather than 80μm) inside the PPLN crystal. This could be achieved through the use of a shorter focal length intracavity lens (40 mm) as shown in Figure 10. However, this approach would reduce cavity length and would not allow for enough space to accommodate all components in the current design, a problem which could be eliminated in the future by having access to more appropriate mounts. This will have to be taken into account when power performance of the system is assessed.

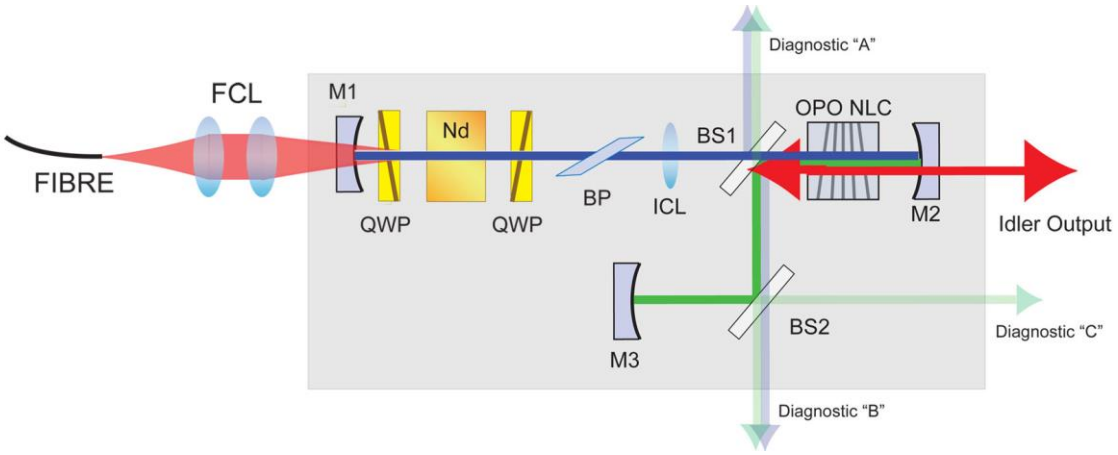

Figure 8: Modified singly-resonant intracavity OPO design with the addition of a second beam splitter (BS2) inside the signal cavity.

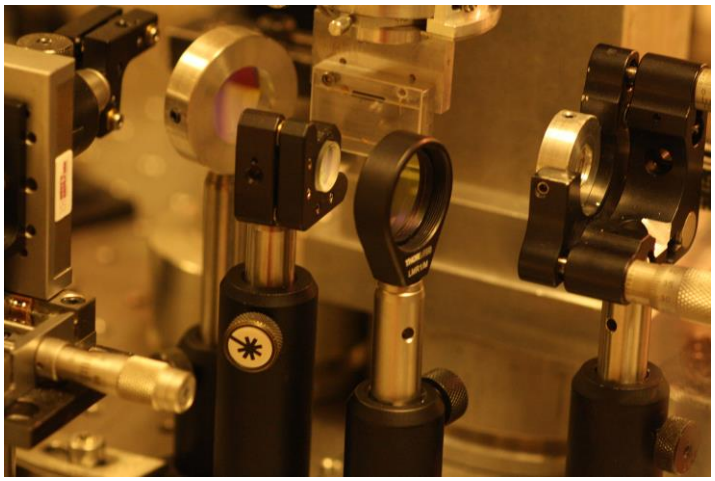

Figure 9: A photograph of the double beam splitter design

With quarter wave plates returned to the 'active' position 93.9mW of idler at a wavelength of 3.2μm was extracted for 3W of diode pump power. The output power tuning characteristic of the now completed OPO is displayed in Figure 11. As expected, the increase in quantum defect caused a drop in idler power at longer wavelengths.

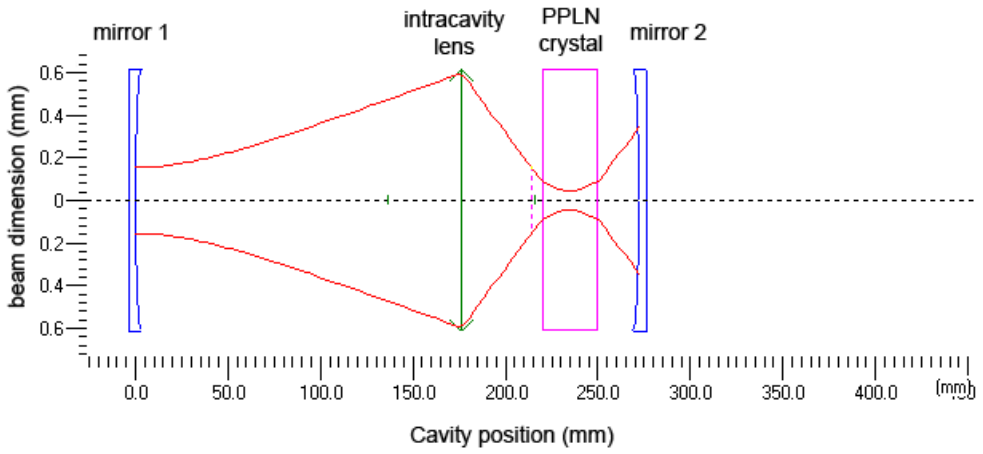

Figure 10: By using a 40 mm focal length intracavity lens, a focal radius of ~40 μm can be achieved inside the PPLN crystal, resulting in an optimised OPO.

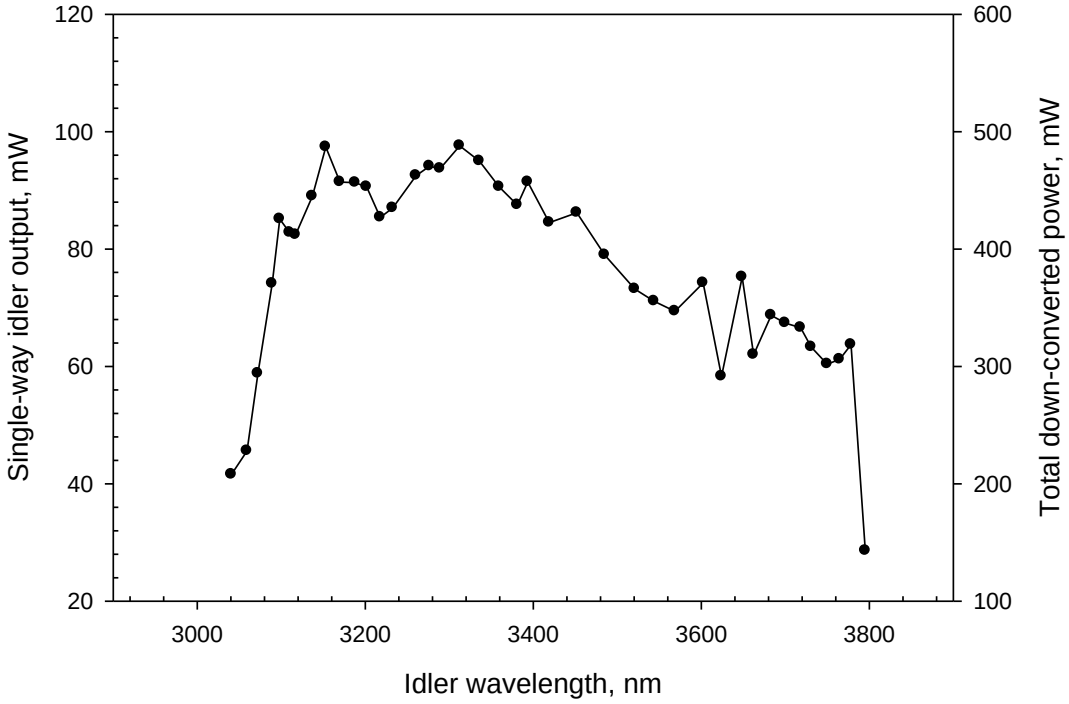

Figure 11: Output power tuning characteristic of the OPO. Idler tuning from 3-3.8μm was achieved by lateral translation of the PPLN crystal. An OSA was used to measure the signal wavelength, from which the idler wavelength was then calculated.

In order to assess whether applying the twisted-mode technique would affect OPO power performance in any way, a comprehensive power-in/power-out analysis was carried out. The results are presented in Figure 12.

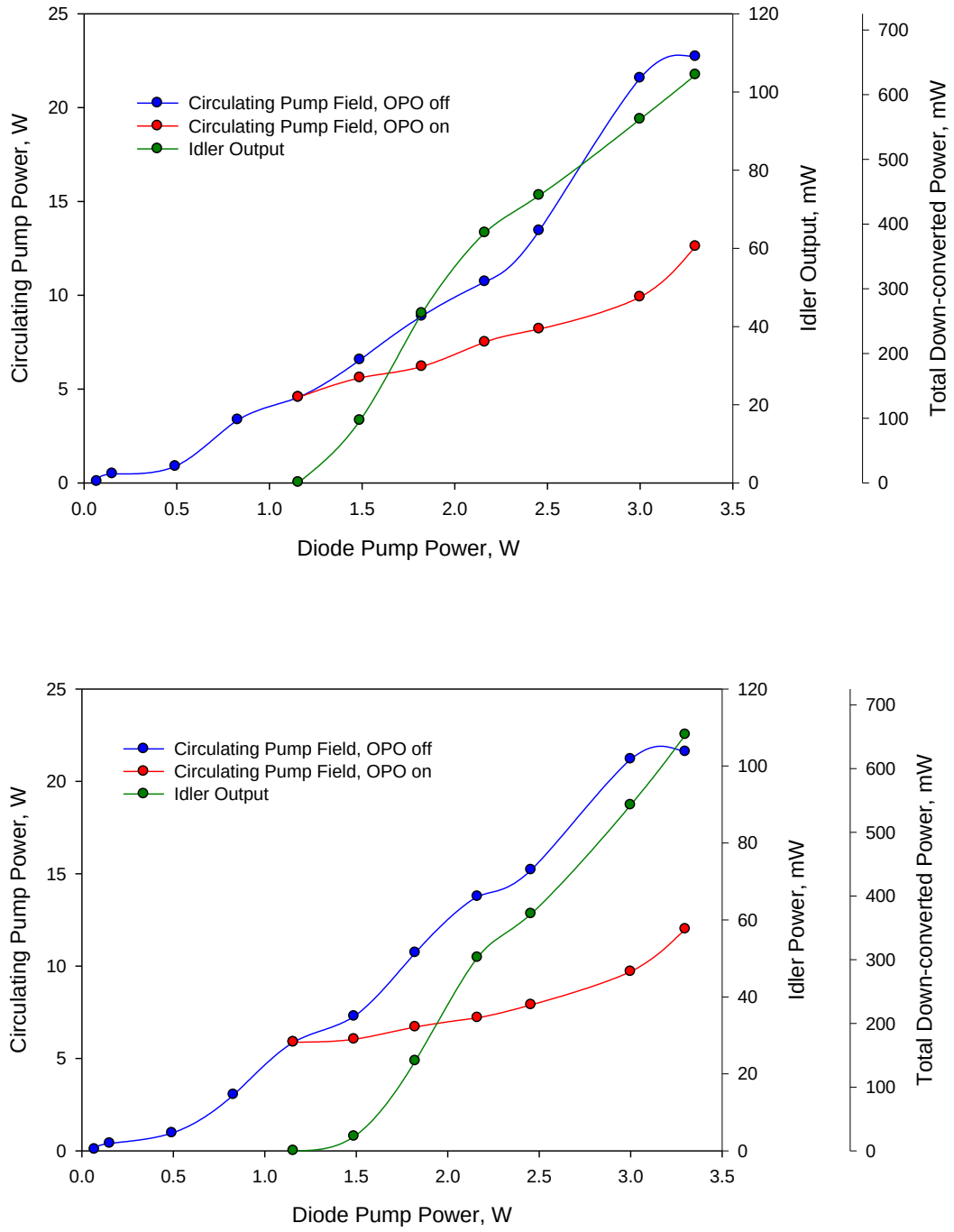

Figure 12: Clamping curves of the OPO. (a) Quarter wave plates in 'active' position. (b) Quarter wave plates in 'neutral' position. Down-conversion efficiencies of ~60% were observed.

It can be seen that the twisted-mode effect had no significant impact on idler output power or pump field clamping behaviour. Both in its presence and absence a down-conversion efficiency of ~60% was achieved, owing to the fact that the pump and signal foci inside the PPLN crystal were not optimised (as discussed above). Down-conversion efficiencies of ~80% could most likely be expected if this problem was rectified.When compared to Figure 3 in chapter two, it is clear that as the diode pumping level is increased, the laser cavity is changed significantly by thermal effects in both the laser gain medium and PPLN crystal, causing a repeatable deviation from the expected horizontal clamping curve when the OPO is operating. Down-conversion efficiencies of ~60% were observed. With the OPO switched off, thermal effects are also evident from the slight (again repeatable) roll-off observed in the circulating pump field at high pumping levels.

Figure 13 shows a summary of OPO power performance for clarity. When optimally output coupled at 10% and pumped at a diode pump level of 3W, the basic laser produced 1.08W of 1 μm light. This dropped to 0.93W upon insertion of the beam splitter and 0.92W upon insertion of the OPO crystal. The 10% output coupler was then replaced with a high reflector and the laser came to threshold at 0.07W of diode pump power. From this we can work out that at a pumping level of 3W, the required OPO threshold for optimal performance is 0.46W of diode pump power. When the OPO was switched on, its observed threshold was 1.157W of diode pump power, meaning the OPO was not optimised. This was confirmed when 93.9mW of idler power was extracted for 3W of diode pump power, corresponding to a total down-converted power of 564mW. This was found to be ~60% of the 1μm power extracted (1.08W) when the basic laser was optimally output coupled. To optimise the system the pump and signal foci inside the PPLN crystal would have to be reduced to 37.3 μm in order to achieve the desired OPO threshold. Efficiencies of ~80% could then be expected.

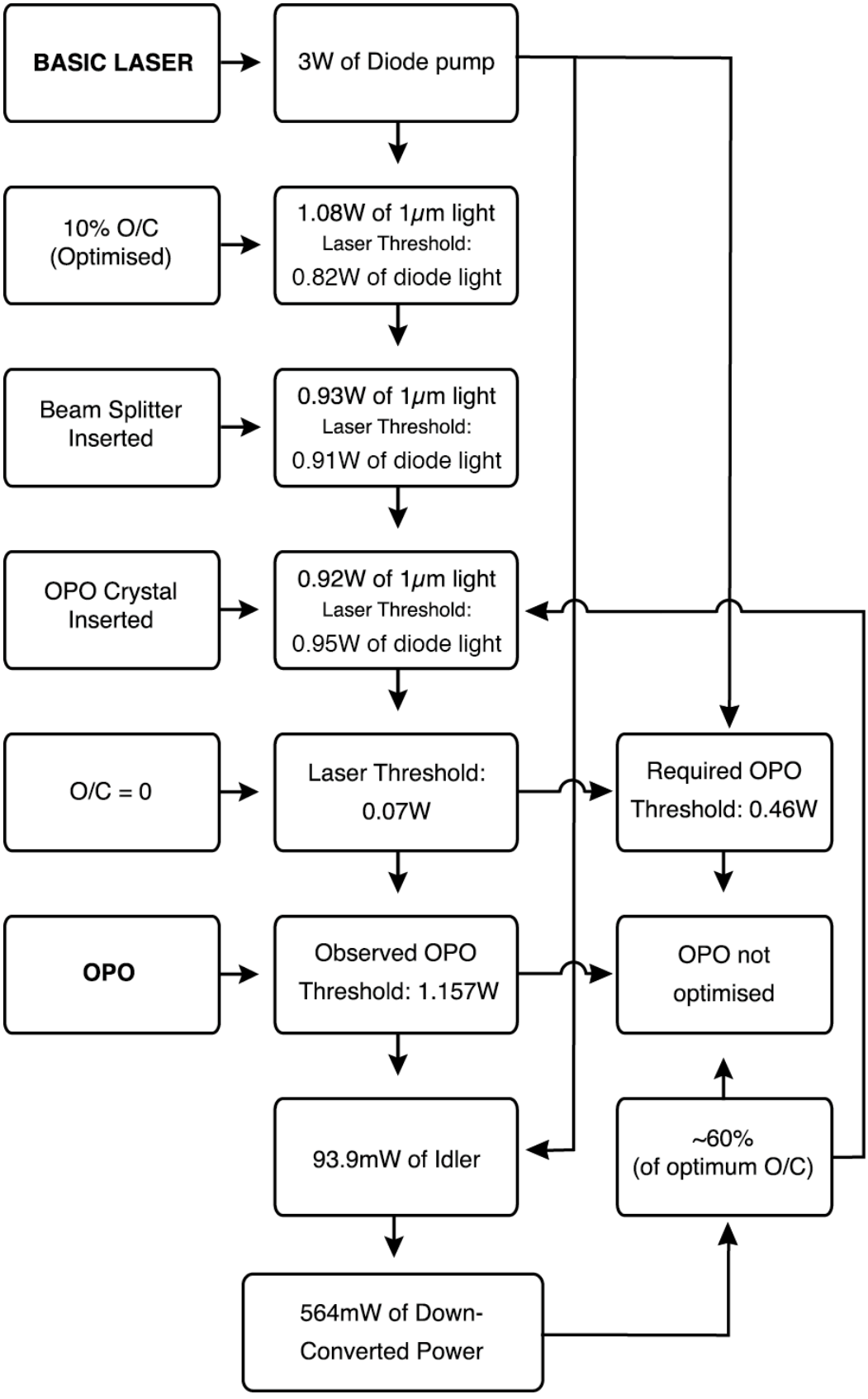

Figure 13: OPO power performance summary.

4.2 Impact of the Twisted-Mode Technique on OPO Frequency Behaviour

To assess the frequency behaviour of both the pump and signal field, a range of diagnostics were set up as shown in Figure 14. The pump field was once again monitored with the help of the two interferometers used previously, while a further confocal interferometer with a free spectral range of 1 GHz was used to analyse the signal field.

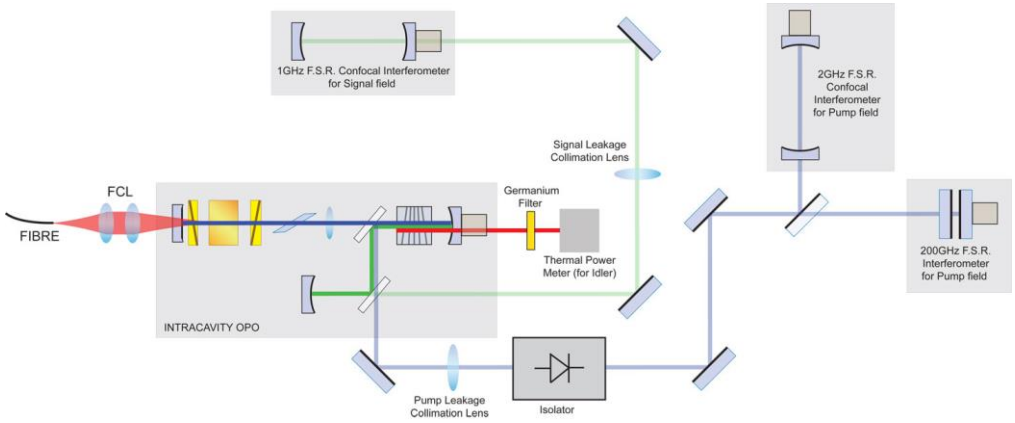

Figure 14: Diagnostic set-up for frequency analysis of pump and signal fields.

As expected, in the absence of the twisted-mode effect the OPO pump field operated on 4-6 longitudinal modes simultaneously due to spatial hole burning and constant erratic mode hopping was observed (Figure 15).

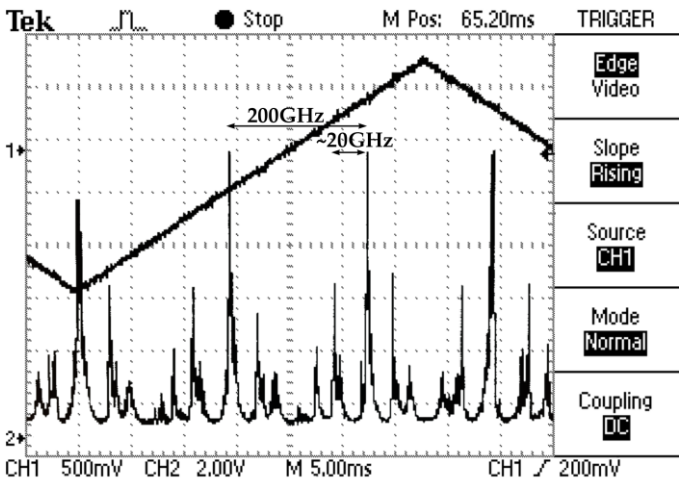

Figure 15: Multi-mode behaviour indicating spatial hole burning in the pump field of the OPO measured on the 200 GHz plane-plane scanning interferometer.

However, this behaviour was much improved when quarter wave plates were turned to the 'active' position. Evidence of this is shown in Figure 16(a)&(b).

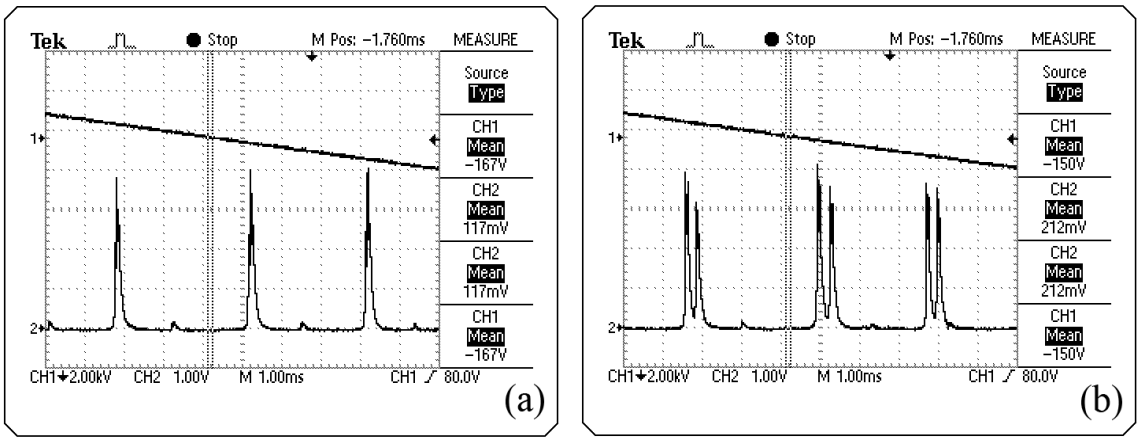

Figure 16: Impact of the twisted mode effect. Both traces were taken with the 200 GHz plane-plane scanning interferometer. The pump field switched continuously between the two behaviours shown.

While single frequency operation occurred only for short periods of time, no more than two modes ever oscillated simultaneously. In order to fully control the pump field an uncoated 1 mm fused silica etalon (150 GHz free spectral range) was inserted into the cavity between the Brewster plate and intracavity lens (the most collimated region of the pump cavity). This caused a 19% drop in idler output power (from 93.9 mW to 76.1 mW), substantially less insertion loss than would be expected in the case of an etalon suppressing spatially hole burnt modes [21]. This is due both to the lower intrinsic loss of the low finesse etalon employed here, as well as the absence of unsaturated regions within the gain material, which occur in etalon narrowed 'traditional' standing wave systems. It should also be noted that the etalon we used had been part of our group's research arsenal for many years and its optical quality was somewhat compromised; the use of a new component with excellent surface quality may further improve power performance of the system. Additionally, while we were sure to place the etalon in the most collimated region of the pump cavity in order to minimise walk-off loss, ideal etalon conditions could not be created during cavity design while also ensuring a good match between pumped and circulating field volumes in the laser gain medium.

Achieving a fully collimated region for etalon placement within the pump cavity by including a second intracavity lens may be an option to be explored at a later date (see Figure 3 in chapter five).

Figure 17 shows the frequency behaviour of the pump field after the insertion of the etalon. Single frequency operation had finally been achieved. Occasional erratic bursts of mode hopping were however still observed. These could be due to the presence of relaxation oscillations or come as a result of the OPO switching on and off as the laser tries to avoid the substantial parametric loss by switching polarisation state. Placing an SHG crystal as well as an extra Brewster plate inside the pump cavity should eliminate both possibilities (see future work).

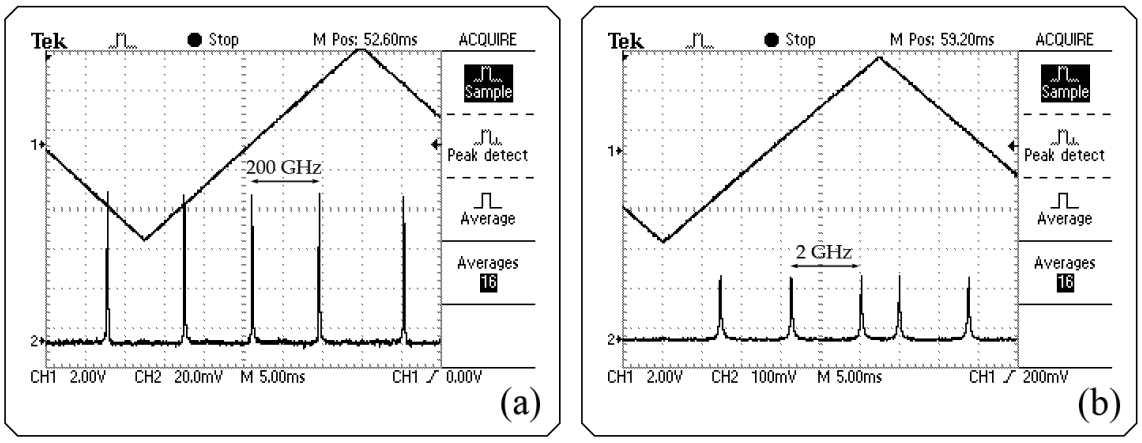

Figure 17: Pump field behaviour after insertion of an uncoated fused silica etalon. Trace (a) was taken with the 200 GHz plane-plane interferometer, while trace (b) was taken with the 2 GHz confocal interferometer. Both interferometers indicate single frequency operation

To guarantee single frequency idler output, both pump and signal fields need to operate on a single-longitudinal-mode. Fortunately, the signal field is not subject to the effects of spatial hole burning and is thus naturally well behaved, oscillating on a single mode (Figure 18). A 50μm silicon etalon (free spectral range of 3THz) was inserted into the signal cavity merely to control mode hopping.

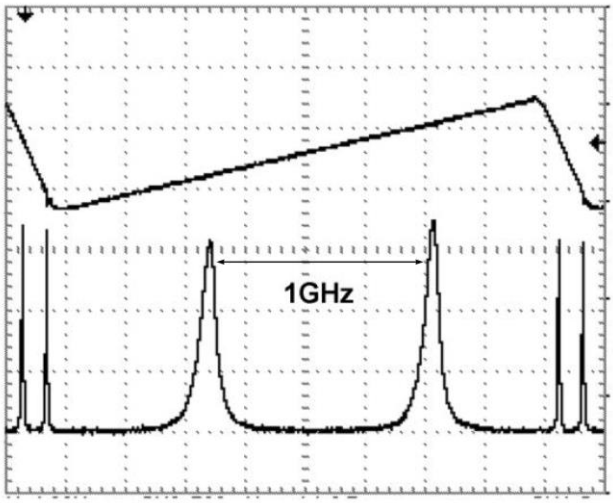

Figure 18: Single frequency operation of the signal field upon insertion of the 50μm silicon etalon. This trace was taken on our 1 GHz confocal scanning interferometer. The next resonating cavity mode would be found ~900 MHz away from the primary mode and would thus be resolved with this interferometer.

4.3 Summary

Our investigation into the elimination of spatial hole burning in the pump field of an intracavity OPO using the twisted-mode technique has proven very fruitful. Implementation of the technique did indeed lead to a substantial improvement in frequency quality of the circulating pump field, which could then be controlled for the most part with the insertion of a low finesse etalon. With the insertion of a further etalon into the signal cavity, single frequency idler output could be achieved. The pump laser and OPO reached threshold at 0.07W and 1.157W of diode pump power respectively, and the twisted-mode effect was not found to impact on the efficiency of the device. At an incident pump power of 3W, 93.9mW of idler was extracted (and ~60% down-conversion efficiencies were achieved). This dropped to a still very respectable 76.1mW after insertion of the etalon into the pump cavity.

Chapter Five: Conclusions

Here we will summarise and review the outcomes of our study into the elimination of spatial hole burning in the pump field of a Nd:YAG based ICOPO by means of the twisted mode technique. Our present findings will be compared to those of a previous investigation conducted by us in 2012, in which a single frequency Nd:YVO_4 ICOPO was achieved with an alternative technique, by inserting etalons into the pump and signal cavities. Which approach proved more favourable in terms of output power and frequency stability? Lastly, future work plans will be discussed, outlining the remaining steps to be taken to enable the realisation of a viable narrow-linewidth mid-IR spectrometer based on ICOPO technology.

5.1 Summary of Results

A basic end-pumped Nd:YAG laser was first created, yielding 1.3W of 1μm output for 3W of diode pump power. Upon insertion of the twisted-mode components (two quarter wave and one Brewster plate) the power level dropped to 1.1W. Power performance was not found to be influenced by the twisted-mode effect; the laser reached threshold at ~0.07W of diode pumping, whether quarter wave plates were turned to the 'active' or the 'neutral' position. The frequency behaviour of the system was however found to be profoundly affected by applying the twisted-mode technique and single frequency operation was able to be achieved effortlessly as seen in Figure 1, which shows once more the oscilloscope traces presented in chapter three. The laser cavity was then extended, using an intracavity lens, in order to accommodate OPO components, which was not found to have any noticeable effects on performance. Once the dichroic beam splitter and PPLN crystal had been included, an output power of 923mW for 3W of incident diode pump power was observed. Frequency behaviour was not found to be impacted, despite the birefringent nature of lithium niobate,

indicating correct alignment of the crystal's fast axis with the linear polarization direction of the pump field.

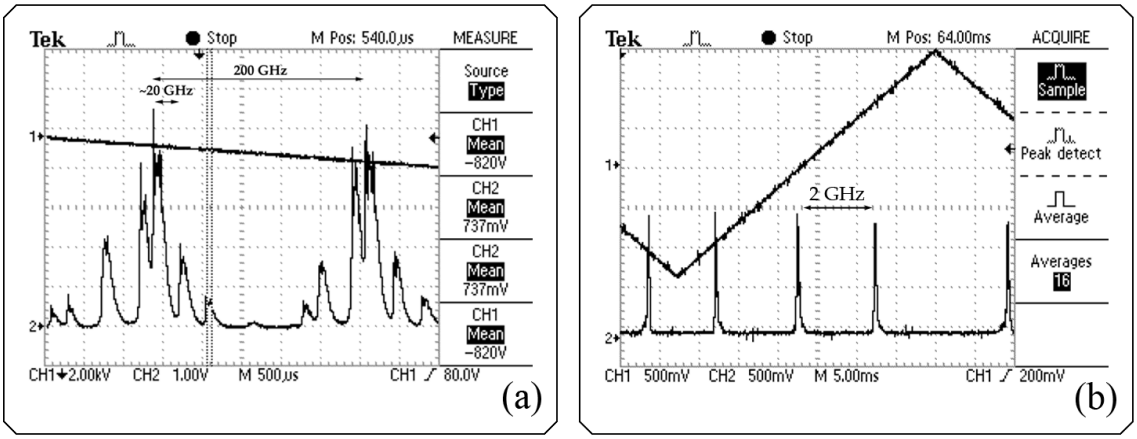

Figure 1: The impact of the twisted-mode technique on the frequency spectrum of the basic laser

Upon completion of the signal cavity using a further beam splitter and outboard end mirror, the OPO reached threshold at ~1.1W of diode pumping and delivered ~94mW of idler output at a wavelength of 3.1µm for 3W of diode pump power. Again applying the twisted-mode technique had no significant impact on power performance. Once more, a substantial linewidth reduction of the pump field was observed when the twisted mode technique was applied and with the inclusion of a low finesse fused silica etalon into the pump cavity single frequency operation was able to be achieved. The relevant traces are shown in Figure 2. While the efficacy of the twisted-mode approach was clearly shown with these results, occasional bursts of multi-mode behaviour accompanied by erratic mode-hopping were still observed. The full potential of this technique with regards to the elimination of spatial hole burning in the pump field of an ICOPO is clearly evident from its tremendous success in the case of the basic 1µm laser. The decrease in frequency stability observed during OPO operation could be attributed to the presence of relaxation oscillations, which are known to cause spectral perturbation in even the most well behaved single frequency laser systems. Alternatively, if the loss experienced by the pump field due to parametric down-conversion exceeds the loss suffered by the wrong polarization state

due to the Brewster plate, the laser would switch polarization and thus prevent OPO operation. Once parametric loss is eliminated in this way, it will be more advantages for the laser to return to its original polarization state. The mode-hopping observed could thus be the result of the OPO switching on and off rapidly. This issue will have to be addressed and plans of action are outlined in the next section.

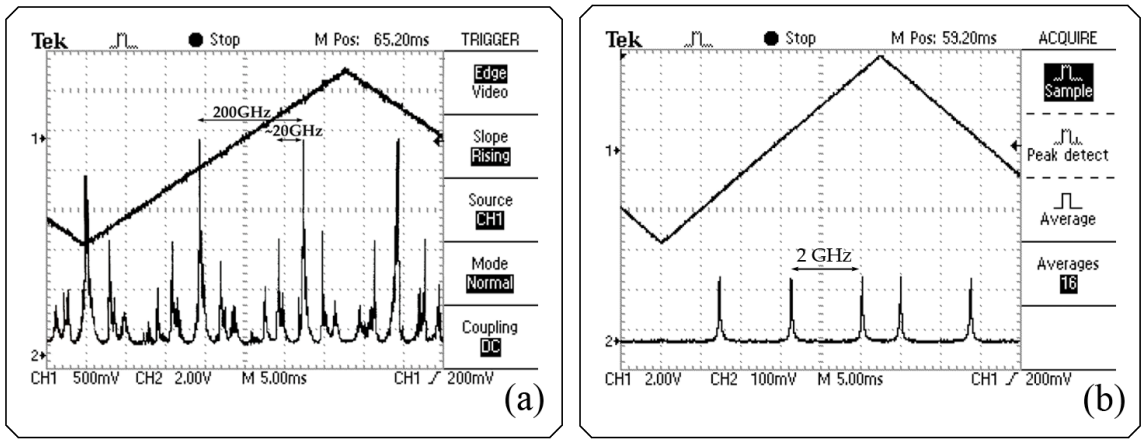

Figure 2: Frequency behaviour of the OPO pump field. Applying the twisted-mode technique and including a low finesse fused silica etalon once again achieved single frequency operation.

Since both pump and signal fields have to operate on a single mode to guarantee single frequency idler output, a 50μm silicon etalon was inserted into the signal cavity in order to control mode hopping and single frequency operation was successfully achieved.

5.2 System Improvement Plans

The above mentioned issue of pump field frequency instability during OPO operation would be the first point to be addressed. Relaxation oscillations of the pump field, whether or not they are to blame for the spectral problem, cause unacceptable fluctuations in idler output amplitude, thus rendering the device unsuitable for most spectroscopic applications. As was shown by us in 2012 [21], the inclusion of an SHG crystal inside the pump cavity of an ICOPO passively eliminates oscillatory behaviour

due to the nonlinear loss experienced by the pump field. Since second harmonic down-conversion is proportional to the square of the fundamental field's intensity, amplitude spikes are 'attacked', while the steady state remains proportionally untouched. This ensures excellent amplitude stability of idler output. If the observed frequency instabilities are not eliminated with this step, further Brewster plates will be inserted into the pump cavity to increase the loss sustained by any unwanted polarization state, giving the laser no choice but to endure parametric down-conversion. Since the inclusion of a PPLN SHG crystal in addition to the OPO crystal will have increased the parametric loss to the pump field, more than one additional Brewster plate may be necessary to achieve this.

Optimisation of OPO down-conversion efficiency is a further future goal. As mentioned in chapter four, using a shorter focal length intracavity lens will tighten the focus in the nonlinear crystal, thus reducing OPO threshold to the appropriate value. However, in order to be able to fit all components inside a shorter pump cavity, the available space will have to be used more efficiently. This could be achieved by mounting the entire laser system on an aluminium mono-block with specially created mounts, a method which was successfully implemented in the Nd:YVO_4 ICOPO built by us in 2012 [21]. As well as being more space-efficient, this approach has the further benefit of over-all improved system stability.

Finally, the lack of a collimated region for etalon placement within the pump cavity will also have to be addressed. One possible solution to be explored is the inclusion of a second intracavity lens between the first lens and the Brewster plate. Provided appropriate focal lengths are chosen, this could create a well collimated pump beam portion, which would minimize etalon walk-off loss, whilst having the added benefit of creating a second focus to accommodate the SHG crystal and at the same time achieving the desired tight focus in the OPO crystal, to ensure optimisation (Figure 3) However, this would involve a substantial increase in pump cavity length, decreasing mode-spacing and mechanical stability.

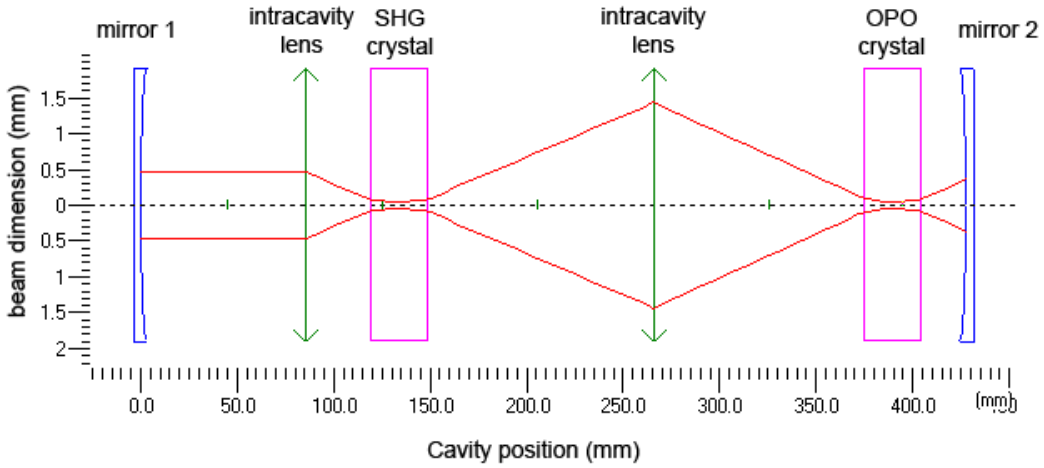

Figure 3: By using two intracavity lenses a collimated region could be realised in the pump cavity for etalon placement. At the same time an appropriately tight focus could be created for each of the nonlinear crystals. In this example created in PSST!, lens 1 and lens 2 have a focal length of 60 mm and 50 mm respectively.

5.3 Comparison between the Nd:YAG and the Nd:YVO_4 system

As previously mentioned a single-frequency mid-IR emitting ICOPO based on the gain material Nd:YVO_4 was realized by us in 2012 [21]. With the insertion of an 80% reflective, 300μm etalon we were able to control the multi-mode behaviour of the pump field very successfully. However, a substantial drop in output power was suffered due to this approach, since the suppression rather than elimination of spatially hole burnt modes leads to gain unsaturated regions within the active laser medium, which are inaccessible to the oscillating mode. We felt that a less wasteful method of frequency control, such as the twisted-mode technique, would be well worth investigating, since it may yield a system with enhanced power performance. It should be noted however, that despite the considerable loss introduced by the insertion of the etalon, 74mW of idler output for 3W of diode pump power was able to be extracted from the Nd:YVO_4 system. This dropped to a still very respectable 57mW upon insertion and activation of the SHG crystal. The system was found to exhibit stable single frequency operation for minutes at a time, only perturbed by cavity length

drifts, an issue that is faced by any single frequency laser, which can be resolved by locking the laser cavity to a reference cavity (see the 'future work' section).

Since Nd:YVO_4 is a birefringent material, it was an unsuitable gain medium choice for the current investigation and the isotropic material Nd:YAG was selected instead, despite its less favourable $\sigma\tau$ product (where σ is the stimulated emission cross section and τ is the upper state life time) and absorption coefficient, as the reduced output power baseline was expected to be more than compensated for by the improved efficiency of the proposed frequency control approach. When the twisted-mode technique was applied to our Nd:YAG based ICOPO, 94mW of idler output was observed at a pump level of 3W. A low finesse silica etalon was required to completely eliminate multi-mode behaviour of the pump field, leaving us with 76mW. It can thus be seen that the Nd:YAG ICOPO could indeed potentially offer a power advantage over its Nd:YVO4 counter-part, if the system improvements outlined in section 5.2 can be implemented successfully. In terms of frequency behaviour the device was observed to be holding single frequency operation reliably between the occasional bursts of mode-hopping mentioned above. We feel that a final judgment on spectral quality cannot be made until these bursts have been eliminated and any comparison to the Nd:YVO_4 system would be unfair at this stage. If reliable and long-lived single frequency operation can indeed be achieved using the twisted-mode approach in the context of an ICOPO, the extent of the thus gained power advantage will determine whether the undeniable increase of system complexity associated with this approach is a price worth paying, given the intention of commercializing the finished source.

5.4 Future Work

Whichever system is chosen to be taken forward, further work will be required to realize a truly utile and commercially viable mid-IR spectroscopic source. The necessary steps are outlined in this section.

5.4.1 Elimination of pump cavity drift using locking techniques

As mentioned previously, pump cavity drift can disrupt single frequency operation in even the most well behaved laser systems. This problem will be eliminated in our system by locking the pump etalon to the pump cavity and in turn slaving the pump cavity to a fixed reference cavity, such as that of a Fabry-Perot Interferometer.

5.4.2 Smooth tuning of the signal

Extensive tuneability is a highly desirable feature in a spectroscopic source and the ICOPO has unprecedented potential in this regard compared to other mid-IR emitting technologies. The substantial phase-matching bandwidth of PPLN (~1.5 THz.cm) would allow the signal field to be smoothly tuned across hundreds of GHz using a tilting etalon. However, to achieve such a broad tuning range, signal cavity length would have to be variable by tens of μm, which is far beyond the range of piezos. Thus an alternative option, such as the use of counter-rotating Brewster plates, would have to be explored. This approach was tested on a simple Nd:YVO_4 laser during our 2012 study and the set-up that was used is shown in Figure 4. We were able to achieve ~15 GHz of smooth tuning (see Figure 5) but were ultimately limited by etalon walk-off loss. Thus the use of an air-spaced etalon could further extend this tuning range.

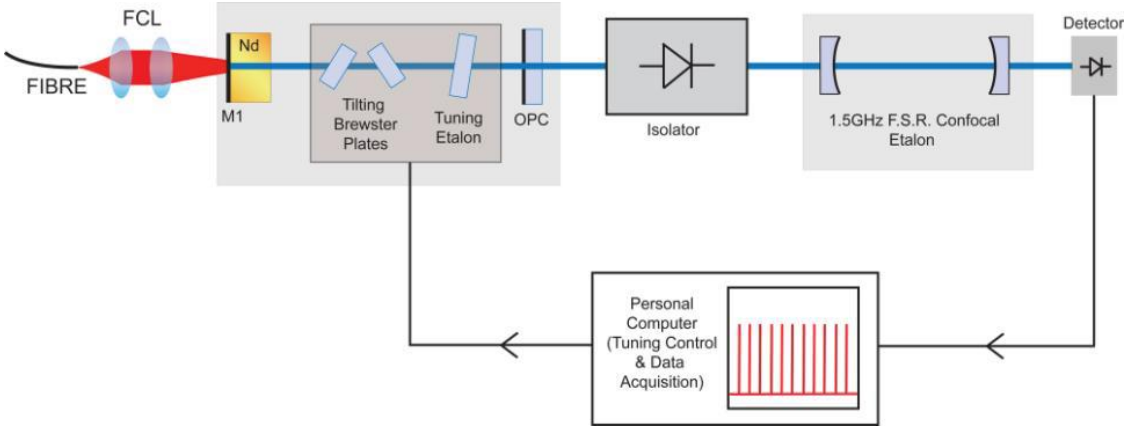

Figure 4: Set-up employed for the smooth tuning of a 1μm laser. The same principle will be applied to the signal cavity of our ICOPO.

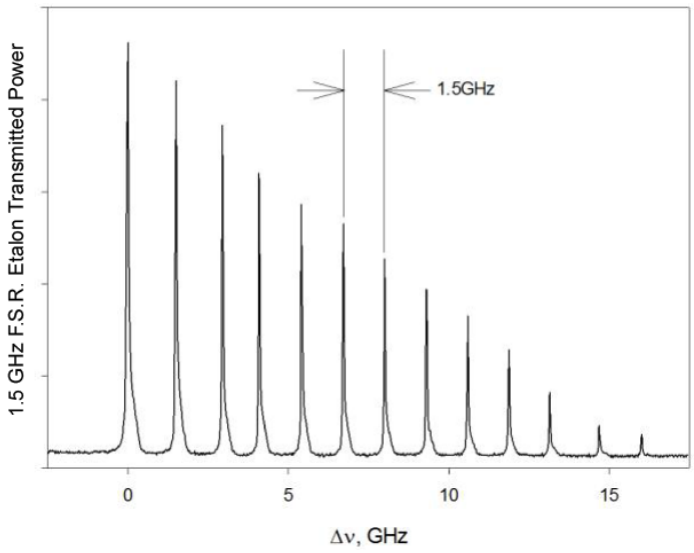

Figure 5: Smooth tuning range resulting from the above set-up, measured using a 1.5 GHz free spectral range static interferometer. The mode-spacing of this 1 μm laser was ~700 MHz, thus multi-mode behaviour would have easily been detected using this et-up.

5.4.3 An ICOPO based spectrometer

Figure 6 shows how an ICOPO based spectrometer might be implemented

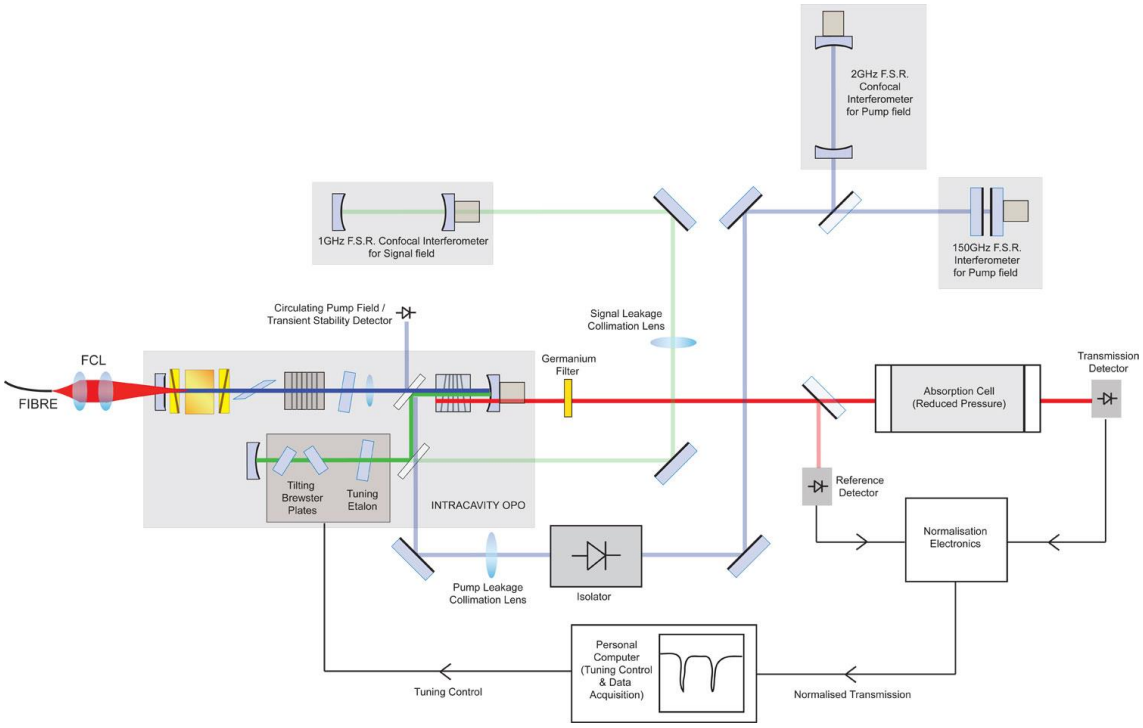

Figure 6: An ICOPO based spectrometer

The locking techniques described above would ensure maximum stability of the fixed-frequency pump field (blue beam), while the signal field (green beam) would be smoothly tuned as discussed in the previous section. A small amount of signal would be picked off at an appropriate diagnostic point, such as the second signal cavity beam splitter, to be passed through a fixed Fabry-Perot Interferometer, resulting in a tuning calibration tool. The idler field (red beam), which can be seen to exit the OPO cavity after a single pass, would be guided into an absorption cell containing some compound to be identified. The unabsorbed light would exit the absorption cell onto a transmission detector, connected to a PC, which would allow us to see key absorption features of the compound inside the cell. In order to compensate for possible idler amplitude fluctuations a small amount of idler would be picked off onto a reference detector before the beam enters the absorption cell, allowing for normalization of the observed transmission.

5.5 Conclusions

In the course of this investigation we have shown that the twisted-mode technique holds great potential for the elimination of multi-mode behaviour in the pump field of an ICOPO. When applied to the basic 1 μm laser, it served to completely suppress spatial hole burning, resulting in effortless single-frequency operation, without impacting on power performance. The laser came to threshold at 0.82 W of diode pump power and 1.063 W of output was extracted at a pumping level of 3 W. Although the spectral quality of the pump field was found to deteriorate somewhat with OPO operation, a vast improvement over the standing-wave configuration was still paramount, once again without a loss in efficiency. 94 mW of idler output were extracted for 3 W of diode pump power and the OPO came to threshold with a circulating pump field of 1.157 W. Down-conversion efficiencies of ~60% were observed. Likely causes for the slight spectral instabilities were able to be identified and will be addressed in future work. Although further research efforts will be required to fully realize the potential of the twisted-mode technique, here we have laid

a solid foundation for future exploration and identified a possible solution to one of the key problems of the solid-state-based Intracavity OPO. An ideal mid-IR spectroscopic source based on ICOPO technology is within reach.

Appendix

Summary of reference [21]

In this study potential solutions to the dual issues of transient instability and multi-longitudinal-mode operation which, have to date hampered the development of continuous-wave (CW), neodymium based Intracavity Optical Parametric Oscillators (ICOPOs) into a viable high resolution spectroscopic source, were explored. An ICOPO based upon the nonlinear material Periodically-poled $LiNbO_3$ (PPLN) was constructed, delivering 160 mW of idler for 3.5W of diode pump when operated ~2 times above threshold. A second, frequency doubling PPLN crystal was placed in the pump-only arm of the cavity in order to suppress the long-lived bursts of relaxation oscillations, which commonly occur in these systems. Whilst this proved successful, a new, low frequency amplitude instability was found to occur at high levels of frequency doubling. This was confirmed to be due to cyclic mode-coupling behaviour within the multi-mode pump field, known as the so-called 'Green Problem' and was eliminated by placing an etalon in the pump cavity and achieving single mode operation. The idler power dropped by ~15% when the frequency doubling suppression effect was maximised, and a further 20% upon insertion of the etalon, resulting in >70mW of single frequency, amplitude stable output in the non-resonant idler field.

References

1 Ngai, A. K. Y. *Spectroscopic applications of continuous wave optical parametric oscillators* PhD thesis, Radboud University, (2008).

2 Hall, R. N., Carlson, R. O., Soltys, T. J., Fenner, G. E. & Kingsley, J. D. Coherent light emission from GaAs junctions. *Phys. Rev. Lett.* **9**, 366-&, doi:10.1103/PhysRevLett.9.366 (1962).

3 Tittel, F., Richter, D. & Fried, A. in *Solid-State Mid-Infrared Laser Sources* Vol. 89 *Topics in Applied Physics* (eds IrinaT Sorokina & KonstantinL Vodopyanov) Ch. 11, 458-529 (Springer Berlin Heidelberg, 2003).

4 Croize, L., Mondelain, D., Camy-Peyret, C., Delmotte, M. & Schmidt, M. Precise measurements of the total concentration of atmospheric CO(2) and (13)CO(2)/(12)CO(2) isotopic ratio using a lead-salt laser diode spectrometer. *Rev. Sci. Inst.* **79**, 9, doi:10.1063/1.2902829 (2008).

5 Werle, P., Slemr, F., Gehrtz, M. & Brauchle, C. Quantum-limited FM-Spectroscopy with a Lead-Salt Diode-Laser - a Comparison of Theoretical and Experimental-Data. *Applied Physics B-Photophysics and Laser Chemistry* **49**, 99-108, doi:10.1007/bf00332268 (1989).

6 Werle, P. *et al.* Near- and mid-infrared laser-optical sensors for gas analysis. *Opt. Lasers Eng.* **37**, 101-114, doi:10.1016/s0143-8166(01)00092-6 (2002).

7 Faist, J. *et al.* Quantum Cascade Laser. *Science* **264**, 553-556, doi:10.1126/science.264.5158.553 (1994).

8 Bai, Y., Bandyopadhyay, N., Tsao, S., Slivken, S. & Razeghi, M. Room temperature quantum cascade lasers with 27% wall plug efficiency. *Appl. Phys. Lett.* **98**, doi:10.1063/1.3586773 (2011).

9 Gmachl, C., Sivco, D. L., Colombelli, R., Capasso, F. & Cho, A. Y. Ultra-broadband semiconductor laser. *Nature* **415**, 883-887, doi:10.1038/415883a (2002).

10 Yao, Y., Hoffman, A. J. & Gmachl, C. F. Mid-infrared quantum cascade lasers. *Nat. Photonics* **6**, 432-439, doi:10.1038/nphoton.2012.143 (2012).

11 Raman, C. V. & Krishnan, K. S. A new type of secondary radiation. *Nature* **121**, 501-502, doi:10.1038/121501c0 (1928).

12 Giordmaine, J. A. & Miller, R. C. Tunable Coherent parametric Oscillation in LiNbO3 at Optical Frequencies. *Phys. Rev. Lett.* **14**, 973-976 (1965).

13 Smith, R. G. *et al.* Continuous optical parametric oscillation in Ba2NaNb5O15. *Appl. Phys. Lett.* **12**, 308-310 (1968).

14 Bosenberg, W. R., A. Drobshoff, J. I. Alexander, L. E. Myers & Byer, R. L. Continuous-wave singly resonant optical parametric oscillator based on periodically poled LiNbO3. *Opt. Lett.* **21**, 713 (1996).

15 Stothard, D. J. M., Lindsay, I. D. & Dunn, M. H. Continuous-wave pump-enhanced optical parametric oscillator with ring resonator for wide and continuous tuning of single-frequency radiation. *Opt. Expr.* **12**, 502-511, doi:10.1364/opex.12.000502 (2004).

16 Kroll, N. M. Parametric amplification in spatially extended media and application to the design of tuneable oscillators at optical frequencies. *Phys. Rev.* **127**, 1207 (1962).

17 Colville, F. G., Dunn, M. H. & Ebrahimzadeh, M. Continuous-wave, singly resonant, intracavity parametric oscillator. *Opt. Lett.* **22**, 75-77 (1997).

18 Lindsay, I. D. *High spatial and spectral quality diode-laser-based pump sources for solid-state lasers and optical parametric oscillators* PhD thesis, University of St Andrews, (1999).

19 Stothard, D. J. M., Ebrahimzadeh, M. & Dunn, M. H. Low pump threshold, continuous-wave, singly resonant, optical parametric oscillator. *Opt. Lett.* **23**, 1895 (1998).

20 Stothard, D. J. M., Dunn, M. H. & Ieee. *Relaxation oscillation suppression in intra-cavity optical parametric oscillators*. (2009).

21 Heering, L. C., Stothard, D. J. M. & Dunn, M. H. in *Photon 12* (eds M. McCall *et al.*) (Institute of Physics, Durham UK, 2012).

22 Edwards, T. J., Turnbull, G. A., Dunn, M. H. & Ebrahimzadeh, M. Continuous-wave, singly-resonant, optical parametric oscillator based on periodically poled KTiOPO4. *Opt. Expr.* **6**, 58-63 (2000).

23 Evtuhov, V. & Siegman, A. E. Twisted-Mode Technique for Obtaining Axially Uniform Energy Density in Laser Cavity. *Appl. Opt.* **4**, 142-143 (1965).

24 Gallaher, N. R. *Narrow Linewidth, Diode Laser Pumped, Solid State Lasers* PhD thesis, University of St Andrews, (1993).

25 Byer, R. L. in *Quantum Electronics: A Treatise* (eds H. Rabin & C.L. Tang) (Academic Press, 1975).

26 Armstrong, J. A., Bloembergen, N., Ducuing, J. & Pershan, P. S. Interactions between Light Waves in a Nonlinear Dielectric. *Phys. Rev.* **127**, 1918 (1962).

27 Ebrahimzadeh, M. & Dunn, M. H. in *Handbook of Optics: Fiber Optics and Nonlinear Optics* Vol. IV (ed M. Bass) Ch. 22, (McGraw-Hill, 1995).

28 Fejer, M. M., G. A. Magel, D. H. Jundt & Byer, R. L. Quasi-Phase-Matched Second Harmonic Generation: Tuning and Tolerances. *IEEE J. Quant. Electron.* **QE-28**, 2631 (1992).

29 Turnbull, G. A., Dunn, M. H. & Ebrahimzadeh, M. Continuous-wave, intracavity optical parametric oscillators: an analysis of power characteristics. *Appl. Phys. B* **66**, 701-710 (1998).

30 Tang, C. L., Demars, G. & Statz, H. Spectral Output and Spiking Behavior of Solid-State Lasers. *J. Appl. Phys.* **34**, 2289-&, doi:10.1063/1.1702732 (1963).

31 Siegman, A. E. *Lasers*. (University Science Books, 1986).